QCD radiative corrections to electroweak-boson production at large transverse momentum in hadron collisions

Richard J. Gonsalves, Jerzy Pawłowski, and Chung-Fai Wai*
Department of Physics and Astronomy, State University of New York at Buffalo, Buffalo, New York 14260
(Received 28 April 1989)

The results of a complete analytical calculation of the next-to-leading-order QCD radiative corrections to the inclusive cross sections parton+parton$\rightarrow V+X$, where V is an on-shell $W^{\pm}$ or Z^0 with transverse momentum Q_T of order M_W, or a massive virtual photon with Q_T of order of its invariant mass, are presented. Numerical predictions for W, Z, and γ^* production at collider energies are also presented. The dependence of the radiative corrections on the choice of renormalization and factorization scales is discussed. The results presented indicate that the QCD-improved parton model can be used to make firm and reliable predictions for electroweak-boson production at large Q_T.

I. INTRODUCTION

The carriers of the weak force, the W and Z bosons, have been observed in proton-antiproton collisions at the CERN S$p\bar{p}$S[1] and Fermilab Tevatron[2] Colliders. These events are probably caused by quark-antiquark annihilations and by radiation off quarks that scatter from other constituents in the colliding hadrons, production mechanisms that are essentially the same as those responsible for "direct" photons and virtual photons which decay to lepton pairs.[3] The cross sections for these processes are sensitive probes of strong-interaction dynamics. Any new massive vector bosons that are not part of the "standard theory" of strong[4] and electroweak[5] interactions as it is presently understood, and which possibly await discovery in hadron-hadron collisions, are likely to be first produced by the same basic mechanism. It is also possible that other types of new particles might be produced in association with electroweak bosons, and most easily observed in such association. It is therefore important to have precise predictions for vector-boson production cross sections within the framework of the standard theory.

The cross sections for vector-boson production by quark-antiquark annihilation are proportional to the electroweak coupling constant α. The QCD radiative corrections to the total production cross sections are of order $\alpha\alpha_s$, where α_s is the QCD coupling strength at a scale on the order of the vector-boson mass, and have been computed.[6] Most bosons produced by this mechanism have very little momentum transverse to the collision axis. To produce a boson with large transverse momentum Q_T costs an additional factor of α_s, evaluated at a scale of order Q_T, required to generate hadrons which balance the transverse momentum. The differential cross section $d\sigma/dQ_T^2$ falls rapidly with Q_T, but it has been measured,[7] and the Q_T dependence provides a more sensitive test of QCD than the total cross section. The radiative corrections of order $\alpha\alpha_s^2$ to large-Q_T production have thus far only been computed for "nonsinglet" cross sections[8] which (essentially) only receive contributions from valence quarks and antiquarks. Nonsinglet corrections dominate at lower energies at which the ratio $\tau=Q^2/S$ of the boson mass squared to the center-of-mass hadron energy squared is not too small. Very roughly, $\sqrt{\tau}$ determines the momentum fraction x of the annihilating partons, while the density of partons with a given x is determined by the energy scale which characterizes the hard-scattering process. In the "Drell-Yan" process at fixed-target energies, only the valence partons are important. However, at the energies $\sqrt{S}\geq 500$ GeV required to produce W's and Z's, the densities of quark-antiquark pairs and of gluons are substantial, and eventually become much larger than valence densities in the multi-TeV energy regime.[9] At CERN Collider energies, for example, quark-gluon scattering accounts for approximately 30% of the cross section at large Q_T. This fraction increases with energy, rising to roughly 50% at 1.8 TeV, and 80% at 40 TeV. Thus it is important to estimate the complete order-α_s^2 corrections at large Q_T (Ref. 10). These corrections determine the scale of α_s and in addition alter the leading-order cross section by a Q_T-dependent "K factor" which can be substantial not only at large Q_T, but also in the "Sudakov" region of small Q_T^2/Q^2.

In this paper we present the results of a complete calculation of the order-α_s^2 corrections to γ^*, $W^{\pm}$, and Z production. We assume that Q_T is of order Q. Thus, while the analytic form of the perturbative cross section in the Sudakov region may be extracted from our results,[11] we do not address the problem[12] of summing large logarithms of Q_T^2/Q^2 in this paper. We also assume that the quarks involved are either effectively massless or sufficiently heavy that they decouple at the relevant energy scales. Thus flavor thresholds are included in an approximate way. In Sec. II we outline the parton-model framework of the calculation and present the general form of the parton-level cross sections with their flavor structure explicitly displayed. In Sec. III we discuss details of the perturbative calculation including the treatment of γ_5 couplings in the context of dimensional regu-

larization. In Sec. IV we present numerical predictions for W, Z, and γ^* production, and discuss the dependence of these predictions on the choice of renormalization and factorization scales. The principal conclusions drawn from these results is that the QCD radiative corrections are small, which indicates that the predictions are firm and reliable. Detailed analytic formulas for all parton-level cross sections are given in the Appendix.

After this calculation was substantially complete, we learned that an independent calculation had also been performed by Arnold and Reno.[13] We have compared our formulas with theirs, and find that all parton-level cross sections presented in their paper agree analytically with the corresponding formulas in this paper. Our calculation includes some additional contributions of order α_s^2 not considered by them. These arise from the two virtual diagrams in Fig. 2 which contain triangular quark loops, and from the interference between diagrams a and b in Fig. 4, and they do make a (numerically) small contribution to Z^0 production in regions between heavy-flavor thresholds.

II. THE HADRONIC CROSS SECTIONS

In this section we define the general structure of the cross sections for inclusive production of an electroweak boson V within the framework of perturbative QCD. The experimental processes for which we will present predictions are

$$h_1(P_1)+h_2(P_2)\rightarrow V(Q)+X \ . \tag{2.1}$$

Here h_i, $i=1,2$ are unpolarized hadrons with momenta P_i, and V stands for an on-shell $W^{\pm}$ or Z^0 with transverse momentum Q_T^2 of order $Q^2=M_V^2$ or a virtual photon with Q_T^2 of order $Q^2 \gg M^2_{\text{hadron}}$.

A. Parton model and kinematics

The QCD-improved parton model predicts that if the intrinsic energy scale involved is sufficiently large, the inclusive cross section for the process (2.1) can be reliably computed using the approximate factorized form

$$E_Q\frac{d\sigma}{d^3Q}=\sum_{a_1,a_2}\int_0^1 dx_2 dx_1 f_{a_1}^{h_1}(x_1,M^2) f_{a_2}^{h_2}(x_2,M^2) E_Q\frac{d\sigma^{a_1a_2}}{d^3Q}(x_1P_1,x_2P_2,M^2) \ . \tag{2.2}$$

Here $E_Q\equiv Q^0$, a and b stand for quarks, antiquarks, or gluons, $f_a^h(x,M^2)$ is the probability density for finding parton a with momentum fraction x in hadron h if it is probed at scale M^2, and $\sigma^{ab}(p_1,p_2,M^2)$ is the perturbative cross section for the process

$$a(p_1)+b(p_2)\rightarrow V(Q)+X \ , \tag{2.3}$$

from which collinear singularities arising from radiation off massless partons have been factorized out at scale M^2 and implicitly included in the scale-dependent parton densities $f_a^h(x,M^2)$ (Ref. 14).

To establish notation and conventions we next specify more precisely how the hard-scattering cross section σ^{ab} depends on the integration variables x_i. We define Mandelstam variables appropriate to the hadron and parton levels as

$$\begin{aligned} &S=(P_1+P_2)^2, \quad T=(P_1-Q)^2, \quad U=(P_2-Q)^2 \ , \\ &s=(p_1+p_2)^2, \quad t=(p_1-Q)^2, \quad u=(p_2-Q)^2 \ , \\ &S_2\equiv S+T+U-Q^2, \quad s_2\equiv s+t+u-Q^2 \ . \end{aligned} \tag{2.4}$$

Here S_2 and s_2 are the invariant masses of the system recoiling against V at the hadron and parton levels, respectively. We will express the hard-scattering cross section σ^{ab} in terms of the variables s, t, u, and s_2, which can in turn be expressed in terms of S, T, U, and Q^2 using $p_i=x_iP_i$.

Following Ref. 8 we make a change of integration variables in Eq. (2.2) to deal with the singular behavior of σ^{ab} in the limit $s_2\rightarrow 0$. These singularities, which are actually integrable, are the remnants of cancellations between nonintegrable singularities due to soft gluon emission in the recoiling parton system and infrared singularities that arise from virtual-gluon exchange. The cancellation, which will be discussed later, produces "+" distributions in the variable s_2 which are to be integrated using the rules

$$\begin{aligned} &\int_0^A ds_2 f(s_2)\left[\frac{1}{s_2}\right]_{A+}=\int_0^A ds_2\frac{f(s_2)-f(0)}{s_2} \ , \\ &\int_0^A ds_2 f(s_2)\left[\frac{\ln(s_2)}{s_2}\right]_{A+} \\ &\qquad =\int_0^A ds_2\frac{[f(s_2)-f(0)]\ln(s_2)}{s_2} \ . \end{aligned} \tag{2.5}$$

These singularities are conveniently handled by the change of variable

$$\begin{aligned} &\int_0^1 dx_1 dx_2\theta(s_2)\theta(p_1^0+p_2^0-Q^0) \\ &\qquad =\int_B^1\frac{dx_1}{x_1S+U-Q^2}\int_0^A ds_2 \ , \end{aligned} \tag{2.6}$$

where

$$A=U+x_1(S_2-U), \quad B=\frac{-U}{S_2-U} \ . \tag{2.7}$$

B. Contributing parton subprocesses

Let us first define the various standard-theory coupling constants and other parameters. The vertex describing the emission of an electroweak boson V by a quark with flavor $f_1=u,d,s,c,b,\ldots$ which then changes to f_2 is described by the Feynman rule

$$-ie\gamma^{\mu}\left[L_{f_2f_1}\frac{1-\gamma_5}{2}+R_{f_2f_1}\frac{1+\gamma_5}{2}\right], \tag{2.8}$$

where the left- and right-handed couplings L and R are

$$\begin{aligned}
&W^-\text{:}\ L_{f_2f_1}=\frac{1}{\sqrt{2}\sin\theta_W}(\tau_+)_{f_2f_1}U_{f_2f_1},\quad R_{f_2f_1}=0\ ,\\
&W^+\text{:}\ L_{f_2f_1}=\frac{1}{\sqrt{2}\sin\theta_W}(\tau_-)_{f_2f_1}U^{\dagger}_{f_2f_1},\quad R_{f_2f_1}=0\ ,\\
&Z^0\text{:}\ L_{f_2f_1}=\frac{1}{\sin 2\theta_W}(\tau_3)_{f_2f_2}-\delta_{f_2f_1}e_{f_1}\tan\theta_W\ ,\\
&\qquad R_{f_2f_1}=-\delta_{f_2f_1}e_{f_1}\tan\theta_W\ ,\\
&\text{Photon:}\ L_{f_2f_1}=R_{f_2f_1}=\delta_{f_2f_1}e_{f_1}\ ,
\end{aligned} \tag{2.9}$$

where $\theta_W=28.4°$ is the electroweak mixing angle, e_f the fractional electric charge of the quark ($e_f=\frac{2}{3}$ for u,c,t and $-\frac{1}{3}$ for d,s,b), $\tau_{\pm}=(\tau_1\pm i\tau_2)/2$, and τ_3 are weak-isospin Pauli matrices, and U is the unitary Cabibbo-Kobayashi-Maskawa mixing matrix. We shall often abbreviate $L_{f_2f_1}$ to L_{21}, etc. The coupling of a quark to a gluon is described by the Feynman rule

$$-ig\gamma^{\mu}t_c\ , \tag{2.10}$$

where the color matrices t_c and number of colors N_c are related to C_F and C_A, the Casimir operators in the fundamental and adjoint representations of SU(N_c), by

$$\begin{aligned}
&N_c=C_A,\quad \sum_{c=1}^{N_c^2-1}t_ct_c=C_F=\frac{N_c^2-1}{2N_c}\ ,\\
&\mathrm{Tr}(t_ct_{c'})=\tfrac{1}{2}\delta_{cc'}\ .
\end{aligned} \tag{2.11}$$

Of course, $N_c=3$ for QCD, but all formulas in this paper hold for general N_c.

We next specify the possible parton subprocesses that can contribute to the hadronic cross section through order α_s^2 in QCD perturbation theory, and display the general form of these contributions. The invariant functions in terms of which these general forms are written are somewhat complicated; they are therefore relegated to the Appendix.

1. The Compton process $qG\to V+X$

The inclusive cross section has the form

$$\begin{aligned}
E_Q\frac{d\sigma^{qG}}{d^{n-1}Q}=\frac{\alpha\alpha_s^{\overline{\mathrm{MS}}}(\mu^2)C_F}{s(2\pi\mu^2)^{2\omega}(N_c^2-1)(1+\omega)}\Bigg\{&\delta(s_2)A^{qG}(s,t,u,Q^2)\sum_{f<}(|L_{f1}|^2+|R_{f1}|^2)+\frac{\alpha_s^{\overline{\mathrm{MS}}}(\mu^2)}{2\pi}\frac{\Gamma(1+\omega)}{\Gamma(1+2\omega)}\left[\frac{Q^2}{4\pi\mu^2}\right]^{\omega}\\
&\times\Bigg\{\Bigg[\delta(s_2)\Bigg[B_1^{qG}(s,t,u,Q^2)+B_2^{qG}(s,t,u,Q^2)\sum_{f'<}(1)+C_1^{qG}(s,t,u,Q^2)\Bigg]\\
&+C_2^{qG}(s,t,u,Q^2)\Bigg]\sum_{f<}(|L_{f1}|^2+|R_{f1}|^2)\\
&+\delta(s_2)B_3^{qG}(s,t,u,Q^2)(L_{11}-R_{11})\sum_{f<}(L_{ff}-R_{ff})\Bigg\}\Bigg],
\end{aligned} \tag{2.12}$$

where the function A^{qG} represents the contribution of the lowest-order diagrams in Fig. 1:

$$A^{qG}(s,t,u,Q^2)=-(1+\omega)\left[(1+\omega)\left[\frac{s}{t}+\frac{t}{s}\right]+\frac{2uQ^2}{st}+2\omega\right], \tag{2.13}$$

and the functions B^{qG} and C^{qG}, which represent the contributions of the virtual diagrams in Fig. 2, and the diagrams in Fig. 3, respectively, are given in Eqs. (A4)–(A6) and (A10)–(A12) in the Appendix. $\overline{\mathrm{MS}}$ denotes the modified minimal-subtraction scheme.

The flavor structure of the cross section is explicitly displayed in this expression. The symbol $\sum_{f<}$ stands for a sum over quarks with masses less than an appropriately chosen flavor threshold [e.g., $\sum_{f<}(1)=4$ if the relevant energy scale E_s, to be specified more precisely later, is in the range $m_c=1.5\ \mathrm{GeV}<E_s<m_b=4.5\ \mathrm{GeV}$]. This is a crude way of taking the masses of heavy quarks into account, having assumed in computing the functions A^{qG}, etc., that all quarks were strictly massless.

In the above expressions, $n=4+2\omega$ is the dimensionality of space-time. We have used dimensional regularization to control both ultraviolet and infrared divergences in this calculation.[15] However, the above expression is completely finite, the infrared divergences having canceled or been factorized out, and the ultraviolet diver-

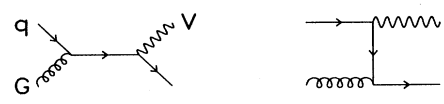

FIG. 1. Diagrams which contribute to the process $qG\to V+X$ in leading order, and give rise to the invariant function A^{qG} of Eq. (2.13). Diagrams contributing to $q\bar{q}\to V+X$ are obtained by crossing.

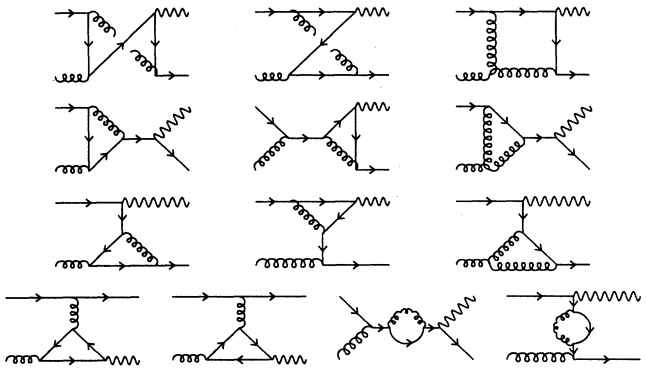

FIG. 2. Diagrams yielding amplitudes whose interference with those of Fig. 1 contribute to the one-loop virtual corrections to $qG \to V+X$, i.e., the functions B^{qG} in Eq. (2.12). The two diagrams with triangular quark loops contribute only to Z^0 production. Renormalization counterterms (not shown) are included with these contributions. Diagrams contributing to $q\bar{q} \to V+X$ are obtained by crossing.

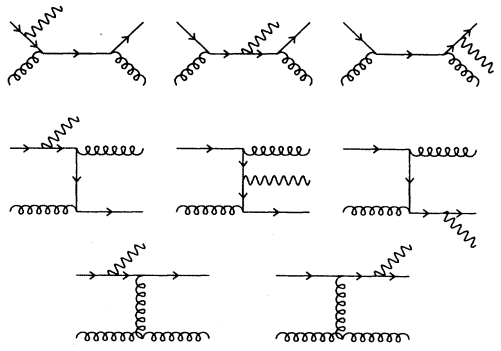

FIG. 3. Diagrams which contribute to the process $qG \to VqG$ and yield the functions C^{qG} in Eq. (2.12). Factorization subtractions are included with these contributions. Diagrams contributing to $q\bar{q} \to VGG$ and $GG \to Vq\bar{q}$ are obtained by crossing.

gences having been absorbed into the bare QCD coupling constant g by use of the $\overline{\text{MS}}$ renormalization prescription[16]

$$\frac{g^2}{4\pi}=\frac{\alpha_s^{\overline{\text{MS}}}(\mu^2)}{\mu^{2\omega}}\left[1+\frac{\alpha_s}{2\pi}\beta_1\left[\frac{1}{\omega}+\gamma_E-\ln(4\pi)\right]\right], \quad (2.14)$$

where $\gamma_E=0.577\,21\ldots$ is Euler's constant,

$$\frac{\alpha_s(\mu^2)}{2\pi}=\frac{1}{\beta_1\ln\left[\frac{\mu^2}{\Lambda^2}\right]}-\frac{\beta_2\ln\ln\left[\frac{\mu^2}{\Lambda^2}\right]}{\beta_1^3\ln^2\left[\frac{\mu^2}{\Lambda^2}\right]},$$

$$\beta_1=\tfrac{11}{6}C_A-\tfrac{1}{3}\sum_{f<}(1), \quad (2.15)$$

$$\beta_2=\tfrac{17}{6}C_A^2-(\tfrac{5}{6}C_A+\tfrac{1}{2}C_F)\sum_{f<}(1),$$

and Λ is the QCD scale parameter that must be determined from experiment. Thus the limit $\omega \to 0$ may be taken in Eq. (2.12), but we have retained various features of the n-dimensional form to establish notation and conventions. The renormalization scale μ is in principle unrelated to the factorization scale M. In practice, both μ and M should be chosen to be of order of the typical energy scale involved in the process in order to minimize the effect of large logarithms of energy-scale ratios in higher orders. The effect of various choices of M and μ will be discussed in connection with our numerical predictions.

The cross sections for three closely related processes can be obtained directly from Eq. (2.12) with the following replacements:

$$\begin{aligned} &Gq \to V+X: \quad t \leftrightarrow u, f_1 \to f_2, \\ &\bar{q}G \to V+X: \quad L \leftrightarrow -R^\dagger, \\ &G\bar{q} \to V+X: \quad t \leftrightarrow u, \quad f_1 \to f_2, \quad L \leftrightarrow -R^\dagger. \end{aligned} \quad (2.16)$$

2. Gluon-gluon fusion $GG \to V+X$

This subprocess has a relatively simple flavor structure:

$$E_Q\frac{d\sigma^{GG}}{d^{n-1}Q}=\frac{\alpha\alpha_s^{\overline{\text{MS}}}(\mu^2)N_cC_F}{s(2\pi\mu^2)^{2\omega}(N_c^2-1)^2(1+\omega)^2}\left[\frac{\alpha_s^{\overline{\text{MS}}}(\mu^2)}{2\pi}\frac{\Gamma(1+\omega)}{\Gamma(1+2\omega)}\left[\frac{Q^2}{4\pi\mu^2}\right]^\omega\right]$$

$$\times[C^{GG}(s,t,u,Q^2)+C^{GG}(s,u,t,Q^2)]\sum_{f<}\sum_{f'<}(|L_{ff'}|^2+|R_{ff'}|^2). \quad (2.17)$$

The function C^{GG} is given in Eq. (A13). We note that the factor of $(1+\omega)^2$ in this formula arises from averaging over the polarization states of the initial gluons: we have consistently used the convention that a gluon has $n-2=2(1+\omega)$ polarization states in n-dimensional space-time.

3. Quark-antiquark annihilation and scattering $q\bar{q} \to V+X$

These processes receive contributions from the diagrams of Figs. 2, 3, and 4. The inclusive cross section through order α_s^2 has the general form

$$
\begin{aligned}
E_Q \frac{d\sigma^{q\bar{q}}}{d^{n-1}Q} = \frac{\alpha\alpha_s^{\overline{\rm MS}}(\mu^2)C_F}{s(2\pi\mu^2)^{2\omega}N_c} \Bigg[& \delta(s_2) A^{q\bar{q}}(s,t,u,Q^2)(|L_{21}|^2+|R_{21}|^2) \\
& + \frac{\alpha_s^{\overline{\rm MS}}(\mu^2)}{2\pi} \frac{\Gamma(1+\omega)}{\Gamma(1+2\omega)} \left[\frac{Q^2}{4\pi\mu^2} \right]^{\omega} \\
& \times \Bigg\{ \Bigg[\delta(s_2) \Bigg[B_1^{q\bar{q}}(s,t,u,Q^2)+C_1^{q\bar{q}}(s,t,u,Q^2)+[B_2^{q\bar{q}}(s,t,u,Q^2)+D_{aa}^{(0)}(s,t,u,Q^2)] \sum_{f<} 1 \Bigg] \\
& \quad + C_2^{q\bar{q}}(s,t,u,Q^2)+C_2^{q\bar{q}}(s,u,t,Q^2) \\
& \quad + [D_{aa}(s,t,u,Q^2)+D_{aa}(s,u,t,Q^2)] \sum_{f<} 1 \Bigg] (|L_{21}|^2+|R_{21}|^2) \\
& + [\delta(s_2) B_3^{q\bar{q}}(s,t,u,Q^2)+D_{ab}(s,t,u,Q^2) \\
& \quad + D_{ab}(s,u,t,Q^2)] \delta_{12}(L_{11}-R_{11}) \sum_{f<} (L_{ff}-R_{ff}) \\
& + [D_{bb}(s,t,u,Q^2)+D_{bb}(s,u,t,Q^2)] \delta_{12} \sum_{f<} \sum_{f'<} (|L_{ff'}|^2+|R_{ff'}|^2) \\
& + [D_{ac}(s,t,u,Q^2)+D_{ad}(s,t,u,Q^2)](|L_{21}|^2+|R_{21}|^2) \\
& + [D_{bc}(s,t,u,Q^2)\delta_{12}+D_{cc}(s,t,u,Q^2)] \sum_{f<} (|L_{f1}|^2+|R_{f1}|^2) \\
& + [D_{bd}(s,t,u,Q^2)\delta_{12}+D_{dd}(s,t,u,Q^2)] \sum_{f<} (|L_{2f}|^2+|R_{2f}|^2) \\
& + [D_{cd}^{LL}(s,t,u,Q^2)+D_{cd}^{LL}(s,u,t,Q^2)](L_{11}L_{22}+R_{11}R_{22}) \\
& + [D_{cd}^{LR}(s,t,u,Q^2)+D_{cd}^{LR}(s,u,t,Q^2)](L_{11}R_{22}+R_{11}L_{22}) \Bigg\} \Bigg] ,
\end{aligned}
\tag{2.18}
$$

where

$$
A^{q\bar{q}}(s,t,u,Q^2) = -A^{qG}(u,t,s,Q^2) . \tag{2.19}
$$

The functions $D(s,t,u,Q^2)$ in this expression represent contributions from the diagrams of Fig. 4. The subscripts further identify the particular diagrams involved: for example, D_{ab} represents a contribution from the interference of the diagrams labeled a and b in the figure. The analytic forms of all functions in Eq. (2.18) can be found in Eqs. (A7)–(A9) and (A14)–(A27) in the Appendix.

The cross section for the process in which quark and antiquark are interchanged can be obtained from Eq. (2.18) quite simply as

$$
\bar{q}q \to V+X: \quad L \leftrightarrow -R^{\dagger} . \tag{2.20}
$$

4. *Quark-quark scattering* $qq \to V+X$

The contributions from the diagrams in Fig. 5 take the general form

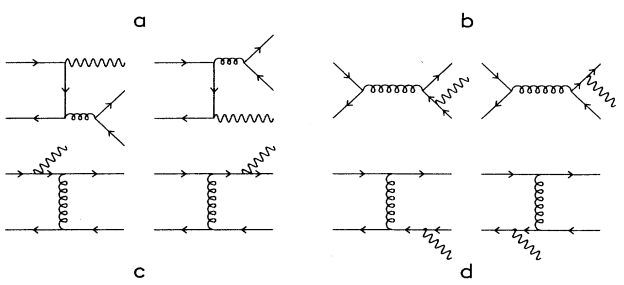

FIG. 4. Diagrams which contribute to the process $q\bar{q} \to Vq\bar{q}$ and yield the functions D in Eq. (2.18).

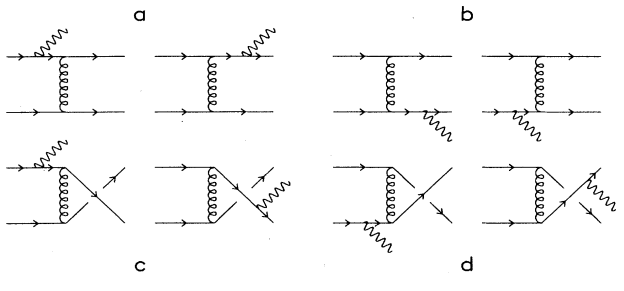

FIG. 5. Diagrams which contribute to the process $qq \to Vqq$ and yield the functions E in Eq. (2.21).

$$E_Q\frac{d\sigma^{qq}}{d^{n-1}Q}=\frac{\alpha\alpha_s^{\overline{\rm MS}}(\mu^2)C_F}{s(2\pi\mu^2)^{2\omega}N_c}\left[\frac{\alpha_s^{\overline{\rm MS}}(\mu^2)}{2\pi}\frac{\Gamma(1+\omega)}{\Gamma(1+2\omega)}\left[\frac{Q^2}{4\pi\mu^2}\right]^{\omega}\right]$$
$$\times\tfrac{1}{2}\Bigg[[E_{aa}(s,t,u,Q^2)+E_{cc}(s,t,u,Q^2)]\sum_{f<}(|L_{f1}|^2+|R_{f1}|^2)$$
$$+[E_{bb}(s,t,u,Q^2)+E_{dd}(s,t,u,Q^2)]\sum_{f<}(|L_{2f}|^2+|R_{2f}|^2)$$
$$+E_{ac}(s,t,u,Q^2)(|L_{21}|^2+|R_{21}|^2)$$
$$+E_{bd}(s,t,u,Q^2)(|L_{12}|^2+|R_{12}|^2)$$
$$+[E_{ad}(s,t,u,Q^2)+E_{bc}(s,t,u,Q^2)]\delta_{12}\sum_{f<}(|L_{f1}|^2+|R_{f1}|^2)$$
$$+[E_{ab}^{LL}(s,t,u,Q^2)+E_{ab}^{LL}(s,u,t,Q^2)](L_{11}L_{22}+R_{11}R_{22})$$
$$+[E_{ab}^{LR}(s,t,u,Q^2)+E_{ab}^{LR}(s,u,t,Q^2)](L_{11}R_{22}+R_{11}L_{22})$$
$$+[E_{cd}^{LL}(s,t,u,Q^2)+E_{cd}^{LL}(s,u,t,Q^2)](L_{11}L_{22}+R_{11}R_{22})$$
$$+[E_{cd}^{LR}(s,t,u,Q^2)+E_{cd}^{LR}(s,u,t,Q^2)](L_{11}R_{22}+R_{11}L_{22})\Bigg]\,. \tag{2.21}$$

The factor of $\frac{1}{2}$ on the second line in this formula is a statistical factor: since we have integrated over the full phase space of the two final-state quarks and summed over all of their quantum numbers, we must divide by 2 to avoid counting each distinct event twice. [An analogous factor for final-state gluons has implicitly been included in the functions $C^{q\bar{q}}$ in Eq. (2.18).] The functions E are given in Eqs. (A28)–(A35).

The cross section for the process in which the quarks are replaced by antiquarks can be obtained from Eq. (2.21) as

$$\bar{q}\,\bar{q}\to V+X:\ \ L\leftrightarrow -R^{\dagger}\,. \tag{2.22}$$

III. THE PERTURBATIVE CALCULATION

In this section we describe the methods used to calculate the parton-level hard-scattering cross sections. For the most part we have followed the procedures used by Ellis, Martinelli, and Petronzio[8] to compute the nonsinglet contributions to the production of lepton pairs at large transverse momentum. In particular we adopt their use of dimensional regularization to control ultraviolet and infrared divergences in intermediate stages of the calculation. Since we have also to deal with W and Z bosons which have parity-violating couplings, we have had to address, in addition, questions relating to the treatment of the Dirac matrix γ_5 in the context of dimensional regularization.

A. Dimensional regularization

Continuing the dimensionality of space-time to $n=4+2\omega$ provides one of the most convenient and efficient ways of regulating both ultraviolet and infrared divergences in a perturbative calculation.[15] Since the technique is well known we will not describe it in detail here. For the virtual diagrams of Fig. 2 we have followed essentially the same procedures as have been used[17] to compute the one-loop corrections to the process $e^+e^-\to q\bar{q}G$. For the real emission diagrams, we have followed closely the procedure described in Appendix B of Ref. 8.

For completeness we describe briefly the procedure used to treat soft singularities, i.e., poles in the variable s_2 that occur in some of the real emission diagrams. The invariant phase space of the parton pair recoiling against the vector boson in the process

$$a(p_1)+b(p_2)\to V(Q)+c(p_3)+d(p_4)\,, \tag{3.1}$$

can be written in the form

$$\int\frac{d^{n-1}p_3\,d^{n-1}p_4}{(2\pi)^{2n-2}4E_3E_4}(2\pi)^n\delta^n(p_1+p_2-Q-p_3-p_4)$$
$$=\frac{\pi^{\omega}s_2^{\omega}\theta(s_2)\Gamma(1+\omega)}{8\pi(2\pi)^{2\omega}\Gamma(2+2\omega)}\int\frac{d\hat{\mathbf{p}}_3}{\Omega_{n-1}}\,, \tag{3.2}$$

where $d\hat{\mathbf{p}}_3$ represents an integration over $n-2$ angles which specify the direction of $\mathbf{p}_3$, and Ω_{n-1} is the surface area of a hypersphere in $(n-1)$-dimensional space. Following Ref. 8 we use the factor of s_2^{ω} in the integration measure to split each pole term in s_2 into a pole in the dimensional regulator ω and integrable distributions in $1/s_2$:

$$s_2^{\omega-1}=\delta(s_2)\left[\frac{1}{\omega}+\ln(A)+\frac{\omega}{2}\ln^2(A)\right]+\left[\frac{1}{s_2}\right]_{A+}$$
$$+\omega\left[\frac{\ln(s_2)}{s_2}\right]_{A+}+O(\omega^2)\,. \tag{3.3}$$

The $A+$ distributions are defined in Eq. (2.5), and the arbitrary quantity A is conveniently chosen to be the upper

limit of the s_2 integral in Eq. (2.6). The pole in ω will cancel an infrared divergence in the virtual-gluon-exchange diagrams.

B. Treatment of γ_5 couplings

It is well known that the Dirac matrix γ_5 cannot be continued to $n \neq 4$ dimensions in a consistent and fully covariant way. It is generally accepted that the noncovariant definition

$$\gamma_5 \equiv i\gamma^0\gamma^1\gamma^2\gamma^3 , \tag{3.4}$$

which was originally proposed by 't Hooft and Veltman,[15] and which implies that γ_5 has the following mixed commutation and anticommutation relations

$$\begin{aligned} &\{\gamma^\mu,\gamma^\nu\}=g^{\mu\nu} , \\ &\{\gamma^\mu,\gamma_5\}=0, \quad \mu \leq 3 , \\ &[\gamma^\mu,\gamma_5]=0, \quad \mu > 3 , \end{aligned} \tag{3.5}$$

does in fact lead to consistent gauge-invariant results,[18] and in particular yields the correct Adler-Bell-Jackiw anomaly.[19]

This noncovariant definition introduces several complications beyond those that one would normally encounter in a calculation with no γ_5 couplings. If, for example, one performs the traces of Dirac matrices before performing the loop integrations in the virtual diagrams, or the phase-space integrations in the real emission diagrams, one encounters noncovariant functions of the integration momenta which are generally much more difficult to integrate than are functions of invariant scalar products of momenta. Since our calculation was originally set up to perform the traces before the integrations, we have adopted the following compromise which we believe must yield the same answers as would the rigorous use of the 't Hooft–Veltman definition.

1. Diagrams involving a single fermion trace

For such diagrams, there exists a simpler and seemingly covariant definition of γ_5 due to Chanowitz, Furman, and Hinchliffe,[20] according to which γ_5 is required to anticommute with all γ^μ. This definition has been shown to yield consistent gauge-invariant results for any gauge-invariant set of diagrams which do not involve the axial anomaly. When the anomaly is present, however, this definition leads to ambiguities which must be resolved by fiat (so as to produce the correct anomalous terms). In the present calculation, there is only one boson with parity-violating couplings. If the diagram involves only one fermion trace, that trace must contain two vertices of the form given in Eq. (2.8). It is easy to show by anticommutation that the real part of the trace is then simply the trace one would obtain for a photon ($L=R=1$) multiplied by $(|L|^2+|R|^2)/2$. The bulk of the calculation involves diagrams of this type.

2. Diagrams involving two fermion traces

These diagrams present a particular problem because the definition of Chanowitz *et al.* has not been shown to be consistently applicable to diagrams with more than one fermion trace. We have therefore computed these diagrams using the 't Hooft–Veltman definition of γ_5. Fortunately, these diagrams are all ultraviolet finite, and suffer from much milder infrared singularities than do the diagrams with a single fermion trace. We have adapted a technique that has been used to compute one-loop radiative corrections in the electroweak theory[21] to perform both the virtual and phase-space integrations. The key ingredient in this technique is to perform the integrations before doing the trace algebra. The integrands are then tensors rather than Lorentz scalars. However, since the noncovariance resides solely in γ_5, the tensors are covariant, and the integrals can be expressed in terms of scalar "form factors" and tensors involving only the fixed external momenta using covariant manipulations. Gauge invariance implies various relations among the form factors and these relations can be used as a check on the calculation. The integrations having been done, the traces involve only the external momenta. The traces are then performed using the noncovariant relations (3.5). Considerable simplifications occur because there are only three independent external momenta, p_1, p_2, and Q, which can be chosen to lie in the 4-dimensional subspace ($\mu=0,1,2,3$) of n-dimensional space.

The virtual diagrams of this type are the two diagrams involving triangular quark loops in Fig. 2. It will be recognized that such loops are responsible for the anomaly. By power counting, each diagram is infrared divergent (if the fermion is massless), as well as ultraviolet divergent. The infrared divergences are actually suppressed if the two gluons attached to the triangle are either on shell or coupled to conserved currents, and the ultraviolet divergences cancel in the sum of the two diagrams. Considerable care must be exercised to bring about these cancellations in a gauge-invariant fashion. We have computed these diagrams using the technique outlined above. In particular we have verified that our manipulations yield the correct anomaly. The contributions of these diagrams are given in Eqs. (A6) and (A9). As a check we have also used the manifestly gauge-invariant and finite result of Adler[19] and Rosenberg[22] for the triangle diagram with a massive fermion in the loop and verified that it yields the same result for the cross section when the mass is set to zero.[23]

The real-emission contributions with two fermion traces arise from the diagrams of Figs. 4 and 5. These are of two types: both γ_5 couplings can occur in one of the traces, in which case the definition of Chanowitz *et al.* can be used to relate the contribution to the cross section for photon production; or, the vector boson V connects the two traces, in which case the 't Hooft–Veltman definition must be used. It turns out that in the case of contributions of the second type, all infrared singularities cancel between contributions from gauge-invariant subsets of diagrams. Nevertheless we have performed a careful calculation of these diagrams in n dimensions using the technique outlined above, and we obtain precisely the same result in the limit $n \to 4$ as is obtained by simply computing these infrared finite contributions in four dimensions. Reference 13 contains an

elegant argument due to Collins that the infrared cancellations occur in any dimensionality close to 4, and that the result should therefore be independent of the precise definition of γ_5: our explicit calculation bears out this general argument.

There appears to be no reason why the 't Hooft–Veltman definition cannot be used to compute all of the other contributions, other than the fact that such a computation is algebraically somewhat tedious. We have performed parts of this calculation. We have also developed n-dimensional generalizations of the Chisholm identities which can be used to simplify the Dirac algebra. A more detailed description of these techniques and the results of the calculation will be given in a separate publication.[24]

C. Factorization of collinear singularities

Finally, we specify the procedure we have used to factorize the residual mass singularities in the perturbative cross sections. This procedure is well known, and we will therefore simply list the factorization subtractions that we have made. These subtractions have been included with the results given in the Appendix for the real-emission diagrams.

1. The Compton process

The real emission diagrams of Fig. 3 have collinear singularities that arise from radiation of a massless parton off either the initial quark or gluon. The initial quark can radiate a collinear gluon and lose a fraction $1-y$ of its momentum. To factorize off the collinear singularity, we add to the perturbative cross section the contribution

$$-\frac{\alpha_s^{\overline{\rm MS}}(\mu^2)}{2\pi}\left[\frac{1}{\omega}+\gamma_E-\ln(4\pi)+\ln\left[\frac{M^2}{\mu^2}\right]\right]\times\int_0^1 dy\, E_Q\frac{d\sigma_{\rm LO}^{qG}(yp_1,p_2)}{d^{n-1}Q}P_{qq}(y)\ . \tag{3.6}$$

Here, $\sigma_{\rm LO}(p_1,p_2)$ is the lowest-order cross section in precisely the form given in Eq. (2.12), and $P_{qq}(y)$ is an Altarelli-Parisi splitting function[25] which gives the probability that the initial quark will have its momentum reduced by the fraction y by emitting a collinear gluon:

$$P_{qq}(y)=C_F\left[\frac{1+y^2}{(1-y)_+}+\frac{3}{2}\delta(1-y)\right]\ . \tag{3.7}$$

Care must be exercised in handling the + distribution in the splitting function. It is defined by the prescription

$$\int_0^1 dy\frac{f(y)}{(1-y)_+}=\int_0^1 dy\frac{f(y)-f(1)}{1-y}\ . \tag{3.8}$$

Since $\sigma_{\rm LO}$ contains a factor

$$\delta((yp_1+p_2-Q)^2)=\delta(u+y(s_2-u))\ , \tag{3.9}$$

we transform the + distribution in y into an $A+$ distribution in s_2 using the identity

$$\frac{1}{(1-y)_+}=(s_2-u)\left[\left[\frac{1}{s_2}\right]_{A+}+\delta(s_2)\ln\left[\frac{A}{s_2-u}\right]\right]\ . \tag{3.10}$$

Finally, we note that since we may write

$$\frac{1}{\omega}+\gamma_E+\ln\left[\frac{M^2}{4\pi\mu^2}\right]=\left[\frac{Q^2}{4\pi\mu^2}\right]^{\omega}\frac{\Gamma(1+\omega)}{\Gamma(1+2\omega)}\left[\frac{1}{\omega}+\ln\left[\frac{M^2}{Q^2}\right]\right]+O(\omega)\ , \tag{3.11}$$

the factorization subtractions do not contribute logarithms of the renormalization scale μ. The procedure described above is generally referred to as $\overline{\rm MS}$ factorization. In principle other factorization schemes[26] may be used. It is straightforward to transform between different schemes. Since we will use parton densities appropriate to $\overline{\rm MS}$ factorization to make numerical predictions, we shall not discuss alternate schemes in this paper.

Collinear singularities in the Compton process will also arise from radiation off the initial-state gluon. This can happen in two ways: the gluon can decay to a $q\bar{q}$ pair and the antiquark with fraction y of the gluon's momentum can annihilate the initial-state quark to produce the vector boson, or the gluon can radiate a gluon and have its momentum reduced by y before participating in the hard scattering. The appropriate factorization subtractions are

$$-\frac{\alpha_s^{\overline{\rm MS}}(\mu^2)}{2\pi}\left[\frac{1}{\omega}+\gamma_E+\ln\left[\frac{M^2}{4\pi\mu^2}\right]\right]\left[\int_0^1 dy\, E_Q\frac{d\sigma_{\rm LO}^{q\bar{q}}(p_1,yp_2)}{d^{n-1}Q}P_{\bar{q}G}(y)+\int_0^1 dy\, E_Q\frac{d\sigma_{\rm LO}^{qG}(p_1,yp_2)}{d^{n-1}Q}P_{GG}(y)\right]\ , \tag{3.12}$$

where the Altarelli-Parisi functions are given by

$$P_{\bar{q}G}(y)=\tfrac{1}{2}[y^2+(1-y)^2]\ , \tag{3.13}$$

$$P_{GG}(y)=2N_c\left[\frac{1}{(1-y)_+}-2+\frac{1}{y}+y(1-y)\right]+\left[\tfrac{11}{6}N_c-\tfrac{1}{3}\sum_{f<}(1)\right]\delta(1-y)\ . \tag{3.14}$$

2. The gluon-gluon process

Collinear singularities arise when either gluon decays to a collinear $q\bar{q}$ pair, and either the quark or the antiquark then hard scatters from the other gluon. The factorization subtractions are

$$-\frac{\alpha_s^{\overline{\rm MS}}(\mu^2)}{2\pi}\left[\frac{1}{\omega}+\gamma_E+\ln\left[\frac{M^2}{4\pi\mu^2}\right]\right]\left[\int_0^1 dy\, E_Q \frac{d\sigma_{\rm LO}^{qG}(yp_1,p_2)}{d^{n-1}Q}P_{qG}(y)+\int_0^1 dy\, E_Q \frac{d\sigma_{\rm LO}^{\bar{q}G}(yp_1,p_2)}{d^{n-1}Q}P_{\bar{q}G}(y)\right.$$
$$\left.+\int_0^1 dy\, E_Q \frac{d\sigma_{\rm LO}^{Gq}(p_1,yp_2)}{d^{n-1}Q}P_{qG}(y)+\int_0^1 dy\, E_Q \frac{d\sigma_{\rm LO}^{G\bar{q}}(p_1,yp_2)}{d^{n-1}Q}P_{\bar{q}G}(y)\right]. \quad (3.15)$$

Charge conjugation implies that $P_{\bar{q}G}=P_{qG}$ in lowest order.

3. Quark-antiquark processes

In the annihilation channel, collinear singularities arise from gluon radiation in the diagrams obtained from those of Fig. 3 by crossing. The factorization subtractions are

$$-\frac{\alpha_s^{\overline{\rm MS}}(\mu^2)}{2\pi}\left[\frac{1}{\omega}+\gamma_E+\ln\left[\frac{M^2}{4\pi\mu^2}\right]\right]\left[\int_0^1 dy\, E_Q \frac{d\sigma_{\rm LO}^{q\bar{q}}(yp_1,p_2)}{d^{n-1}Q}P_{qq}(y)+\int_0^1 dy\, E_Q \frac{d\sigma_{\rm LO}^{q\bar{q}}(p_1,yp_2)}{d^{n-1}Q}P_{\bar{q}\bar{q}}(y)\right]. \quad (3.16)$$

Charge conjugation implies that $P_{\bar{q}\bar{q}}=P_{qq}$ in lowest order. In the scattering channel, singularities arise when the quark or antiquark emits a gluon which then hard scatters from the other parton: the singularities occur in the squares of the diagrams *c* and *d* in Fig. 4. The factorization subtractions are

$$-\frac{\alpha_s^{\overline{\rm MS}}(\mu^2)}{2\pi}\left[\frac{1}{\omega}+\gamma_E+\ln\left[\frac{M^2}{4\pi\mu^2}\right]\right]\times\int_0^1 dy\, E_Q \frac{d\sigma_{\rm LO}^{qG}(p_1,yp_2)}{d^{n-1}Q}P_{G\bar{q}}(y)\,, \quad (3.17)$$

for diagrams *c*, and

$$-\frac{\alpha_s^{\overline{\rm MS}}(\mu^2)}{2\pi}\left[\frac{1}{\omega}+\gamma_E+\ln\left[\frac{M^2}{4\pi\mu^2}\right]\right]\times\int_0^1 dy\, E_Q \frac{d\sigma_{\rm LO}^{G\bar{q}}(yp_1,p_2)}{d^{n-1}Q}P_{Gq}(y)\,, \quad (3.18)$$

for diagrams *d*, where

$$P_{Gq}(y)=P_{G\bar{q}}(y)=C_F\left[\frac{1}{y}+\frac{(1-y)^2}{y}\right]. \quad (3.19)$$

Finally we note that the quark-quark scattering processes which exhibit collinear singularities, i.e., the squares of diagrams *a*, *b*, *c*, and *d* in Fig. 5 are simply related to the quark-antiquark scattering processes, and are rendered finite by subtractions analogous to those in Eqs. (3.17) and (3.18).

IV. NUMERICAL RESULTS AND CONCLUSIONS

In this section we present numerical results for cross sections we believe to be of experimental interest.

A. Assumptions and phenomenological input

1. Parton densities

The most important phenomenological input required in making numerical predictions is a set parton densities $f_a^h(x,M^2)$. We will use the parton distributions of Martin, Roberts, and Stirling[27] (MRS). These distributions have been derived from deeply inelastic scattering data using a full next-to-leading-order analysis based on the $\overline{\rm MS}$ prescription. Unless otherwise noted, we use the MRS set B with $\Lambda_{\overline{\rm MS}}=0.228$ GeV. In evaluating the distributions we take $M^2=Q_T^2$ unless otherwise specified. The MRS set E with $\Lambda_{\overline{\rm MS}}=0.91$ GeV yields cross sections that are roughly 10–20% smaller than does the MRS set B; this difference is generally insignificant given the normalization uncertainties in presently available experimental data.

2. Scale and scheme dependence

The next-to-leading-order cross sections depend on the choice of renormalization and factorization schemes and scales. In this paper we restrict our analysis to the $\overline{\rm MS}$ factorization scheme appropriate to the MRS parton densities. However, within this factorization scheme, we are still free to choose the factorization scale M. This scale should be chosen to be of order of the typical energy scale E_s involved in the hard scattering. The conventional choice of energy scale in large-Q_T production is $E_s^2=Q_T^2$. However, other choices such as the boson mass squared Q^2 or the transverse energy squared $Q^2+Q_T^2$ are possible. Given a choice of E_s we define a factorization scale factor

$$\xi_M\equiv\frac{M^2}{E_s^2}\,. \quad (4.1)$$

In principle, the renormalization scale μ is unrelated to the factorization scale M (Ref. 28). For simplicity we re-

late μ to the same choice of energy scale E_s as M, and define a renormalization scale factor

$$\zeta_\mu \equiv \frac{\mu^2}{E_s^2} . \tag{4.2}$$

It is well known that, in next-to-leading order, a change in renormalization scheme is equivalent to a change in renormalization scale. We generally use the $\overline{\text{MS}}$ scheme in this paper. Alternative schemes are provided by "momentum subtraction,"[29] which is physically somewhat better motivated than $\overline{\text{MS}}$ subtraction. In next-to-leading order, momentum subtraction is equivalent to $\overline{\text{MS}}$ subtraction with a slightly smaller choice of scale. For example, for a momentum-subtraction ("mom") scheme defined so that there are no radiative corrections to the quark-gluon three-point function, $\zeta_\mu^{\text{mom}}=0.21\zeta_\mu^{\overline{\text{MS}}}$. Strategies have been proposed for resolving renormalization-scheme and scale ambiguities, the most noteworthy being the principle of minimal sensitivity,[30] and the method of effective charges.[31]

Two tests that might be applied to decide among the various possible choices of schemes and scales are to find which set of choices yields radiative corrections that are consistently smallest for all values of the kinematic variables, and, of course, which choice yields cross sections that best fit the data. In this paper we will make only a cursory study of scale dependence, leaving a more detailed study of optimizing scheme and scale choices to a future publication.[24]

A technical point related to renormalization-scheme dependence is perhaps appropriately noted here: we use the full next-to-leading-order corrected expression for α_s given in Eq. (2.15) in both the leading- and next-to-leading-order cross-section contributions. In evaluating leading-order (LO) cross sections, however, we use the leading-order expression for α_s.

3. Heavy-quark thresholds

We will also take the masses of heavy quarks (c,b,t) into account in an approximate way by inserting a step function $\theta(E_s^2-4m_f^2)$ into every sum over flavors $\sum_f$. Here E_s is the typical energy scale of the process which we take to equal Q_T unless otherwise specified. We take $m_c=1.5$ GeV, $m_b=4.5$ GeV, and we assume that $m_t=\infty$, i.e., no more than five flavors contribute at any S and E_s. Note that the flavor sums arise both in the real-emission and virtual diagrams. In the real diagrams, $\theta(E_s^2-4m_f^2)$ approximates the threshold factor for heavy-flavor pair production. In the virtual diagrams the step function is supposed to reflect the fact that the heavy quark decouples if the typical external momentum involved is much smaller than its mass.[32] Actually, the only virtual contributions that are affected arise from the renormalization counterterm [i.e., $\sum_{f<}$ in Eq. (2.15)] and the quark-triangle diagrams of Fig. 2 [i.e., the coefficients of B_3 in Eqs. (2.12) and (2.18)]: it should not be too difficult to test the validity of our method of approximating decoupling by including quark masses in these contributions explicitly, but we have not done so. Finally, we do not include explicit flavor threshold factors for initial-state quarks: we assume that these thresholds are built into the parton distributions.

4. Normalization of cross sections

While the QCD-improved parton model predicts the absolute normalization of the inclusive cross section $d\sigma/dQ_T^2$, it is common practice in the literature to present experimental results for ratios of cross sections. This is done partly to minimize the effects of experimental uncertainties, partly to minimize the dependence of the predictions on uncertainties in our knowledge of the structure functions, and also partly because of an apparently widespread belief that this type of process is beset with large and mysterious "K factors." Some of the results we present are therefore normalized to the total cross section. The analytic form of this cross section is known only to order $\alpha\alpha_s$. To this order, only $q\bar{q}$ and qG initial states contribute. The analytic forms of the parton-level cross sections computed using the $\overline{\text{MS}}$ factorization prescription are[33]

$$\sigma^{q\bar{q}}=\frac{2\pi^2\alpha}{sN_c}(|L_{21}|^2+|R_{21}|^2)\left[\delta(1-z)+\frac{\alpha_s}{2\pi}C_F\left\{\left[\frac{2\pi^2}{3}-8-3\ln\left[\frac{M^2}{s}\right]\right]\delta(1-z)\right.\right.$$
$$\left.\left.+4(1+z^2)\left[\frac{\ln(1-z)}{1-z}\right]_+-2\frac{1+z^2}{(1-z)_+}\ln\left[\frac{M^2}{s}\right]\right\}\right], \tag{4.3}$$

where $z=Q^2/s$, and

$$\sigma^{qG}=\frac{2\pi^2\alpha}{s(N_c^2-1)}\sum_{f<}(|L_{f1}|^2+|R_{f1}|^2)\frac{\alpha_s}{2\pi}C_F\left\{[z^2+(1-z)^2]\left[2\ln(1-z)-\ln\left[\frac{M^2}{s}\right]-\frac{3}{2}\right]+2-\frac{z^2}{2}\right\}. \tag{4.4}$$

We will choose the factorization scale $M^2=Q^2$, and use the leading-order expression for α_s [i.e., we set $\mu^2=Q^2$ and $\beta_2=0$ in Eq. (2.15)].

5. Nonsinglet cross sections

In the following we shall often refer to "full" and "nonsinglet" (NS) cross sections. By "full" we mean simply that all possible contributions from valence and sea quarks and from gluons in the colliding hadrons are taken into account. By "nonsinglet" we mean the difference between the cross sections in $p\bar{p}$ and pp collisions:

$$\begin{aligned}&\sigma(p\bar{p}\to W^+ + X)+\sigma(p\bar{p}\to W^- + X)\\&\qquad -\sigma(pp\to W^+ + X)-\sigma(pp\to W^- + X)\ ,\\&\sigma(p\bar{p}\to Z^0 + X)-\sigma(pp\to Z^0 + X)\ ,\\&\sigma(p\bar{p}\to \gamma^* + X)-\sigma(pp\to \gamma^* + X)\ .\end{aligned}\tag{4.5}$$

Loosely speaking, one may think of the nonsinglet cross section as the contribution of the valence quarks in a $p\bar{p}$ collision. However, some valence-valence contributions (e.g., those involving the functions D_{cc} and D_{dd}) drop out of the nonsinglet cross sections as defined above. For W production we add the cross sections for W^+ and W^- to ensure that all valence-sea contributions cancel between the $p\bar{p}$ and pp terms.

B. Numerical results

1. Normalized Q_T distribution

The W transverse-momentum distribution has been measured by the UA1 and UA2 Collaborations at CERN.[7] Their distributions are normalized to the total cross section. In Fig. 6 we compare their data with our results. The three curves in the figure represent theoretical predictions based on the full $O(\alpha_s^2)$ corrected Q_T distribution normalized to the full total cross section with the MRS B and E sets, and the nonsinglet $O(\alpha_s^2)$ corrected distribution normalized to the nonsinglet total cross section with the MRS set B. It is clear that data are consistent with the QCD predictions, but that they are not accurate enough to discriminate between the MRS B and E distributions or between the singlet and nonsinglet theoretical predictions. There is a tantalizing, but statistically insignificant, hint in the data that the experimental cross section might be larger than the theoretical prediction at large values of Q_T. If this potential discrepancy should be confirmed by more accurate measurements, it would represent a firm signal of new physics beyond the standard theory with five flavors.

2. Full and nonsinglet cross sections

In Fig. 7 we compare the "full" Q_T distributions with the "nonsinglet" distributions for W production. Also shown is the leading $O(\alpha_s)$ contribution. The difference between full and NS is due mostly to the quark-gluon Compton process. It is apparent that this difference is quite significant at $\sqrt{S}=1.8$ TeV. Thus if the experimental uncertainties in the normalization of the Q_T distribution could be sufficiently reduced, the absolute distribution could provide striking evidence for the contribution of gluons. The figure also shows that the nonsinglet contribution is slightly harder than the full cross section at very large values of Q_T. Figure 8 compares full and NS distributions for Z^0 production at $\sqrt{S}=1.8$ TeV and 630 GeV. It is apparent that the difference increases significantly with $\sqrt{S}$.

Full and NS distributions (normalized to the full and NS total cross sections, respectively) for γ^* production at $\sqrt{S}=630$ GeV and 63 GeV are shown in Figs. 9 and 10, respectively. At fixed Q_T the normalized cross section increases with the mass Q of the virtual photon. At fixed Q the full and NS cross sections behave similarly to the W and Z cross section in Figs. 6, 7, and 8.

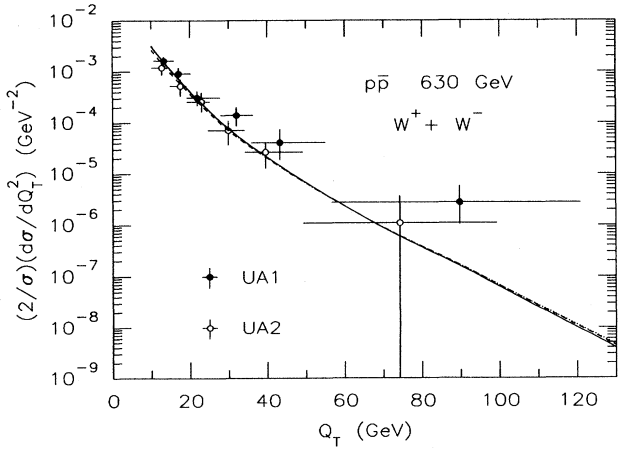

FIG. 6. W production in $p\bar{p}$ collisions at 630 GeV. The solid, dashed, and dotted lines represent the full (MRS B), full (MRS E), and NS (MRS B) predictions. The corresponding total cross sections σ are 5.8, 5.1, and 3.5 nb, respectively.

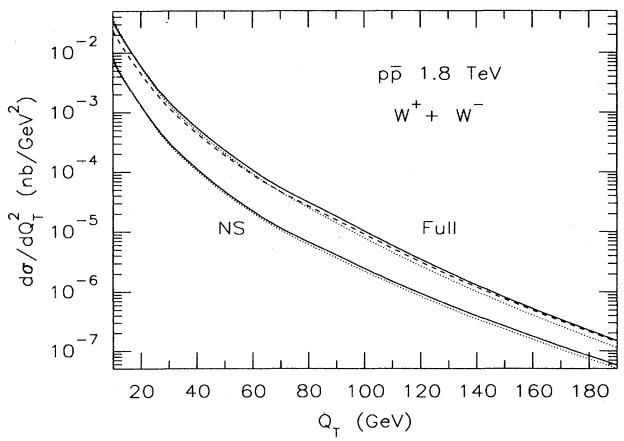

FIG. 7. W production in $p\bar{p}$ collisions at 1.8 TeV. The solid, dashed, and dotted lines represent MRS B, MRS E, and leading-order (MRS B) predictions respectively.

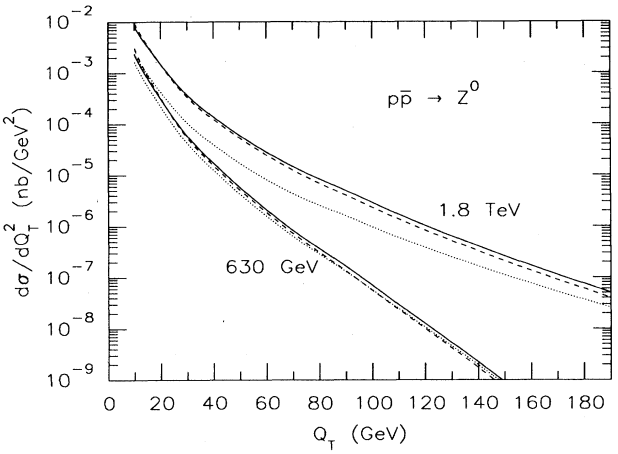

FIG. 8. Z production in $p\bar{p}$ collisions. The solid, dashed, and dotted lines represent full, leading order, and NS contributions, all with the MRS B set.

3. *Relative contributions of quarks and gluons*

In Figs. 11, 12, and 13 we compare the relative contributions of quarks (i.e., qq, $q\bar{q}$, and $\overline{qq}$), of the Compton processes (qG,$\bar{q}G$), and of the gluon-gluon process at $\sqrt{S}=1.8$ TeV, 630 GeV, and 40 TeV, respectively. Shown separately in these figures are the contributions of the leading $O(\alpha_s)$ (LO), and next-to-leading $O(\alpha_s^2)$ (NLO) terms in the cross section. (The curves plotted are smooth curves drawn through a small number of computed points: while they represent the magnitudes and general trends of the cross-section contributions, they should not be taken to represent their precise Q_T dependence.) In general, the separation between LO and NLO is strongly dependent on the renormalization and factorization schemes and scales used, especially at small values of Q_T, and thus it is only the sum of the two that is really

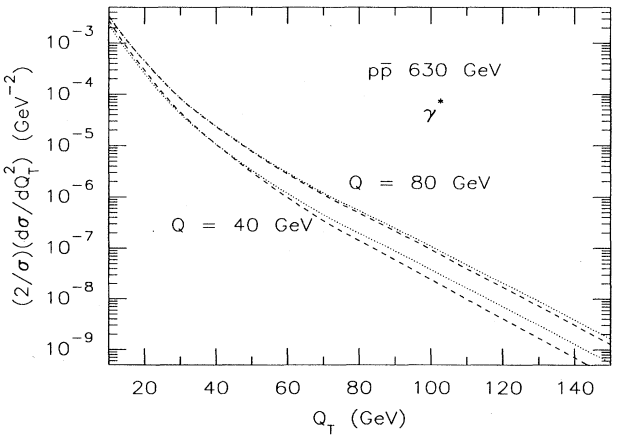

FIG. 9. γ^* production in $p\bar{p}$ collisions at 630 GeV. The dashed and dotted lines represent full and NS contributions, respectively. The corresponding total cross sections (for lepton pair production) are 0.30×10^{-3} and 0.21×10^{-3} pb at $Q=80$, and 8.9×10^{-3} and 4.1×10^{-3} pb at $Q=40$.

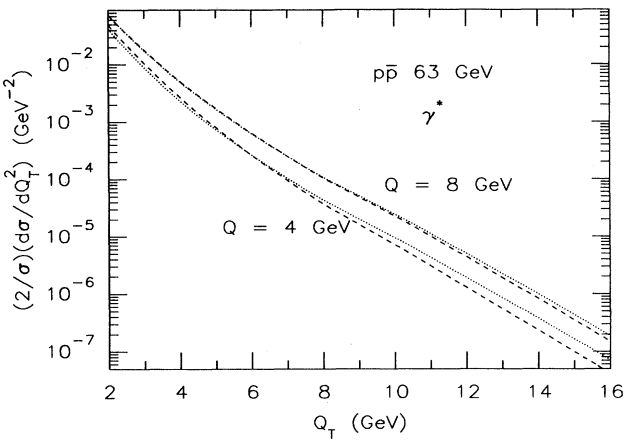

FIG. 10. γ^* production in $p\bar{p}$ collisions at 63 GeV. The dashed and dotted lines represent full and NS contributions respectively. The corresponding total cross sections (for lepton pair production) are 4.0 and 2.8 pb at $Q=8$, and 94 and 46 pb at $Q=4$.

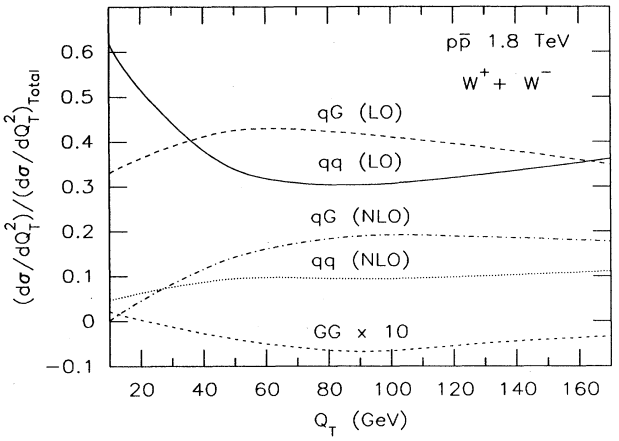

FIG. 11. Relative contributions to W production at 1.8 TeV of $O(\alpha_s)$ (LO) and $O(\alpha_s^2)$ (NLO) terms in the cross section from processes with no initial-state gluons (qq), one initial-state gluon (qG), and two gluons (GG).

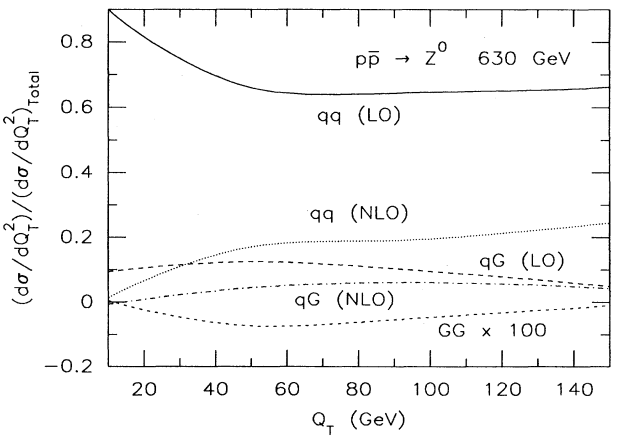

FIG. 12. Same as Fig. 11, but for Z^0 production at 630 GeV.

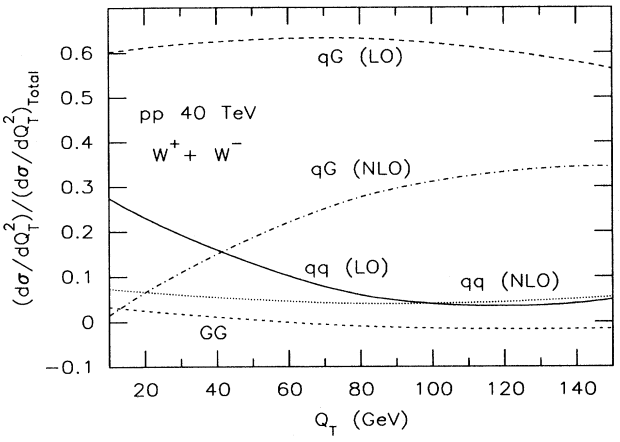

FIG. 13. Same as Fig. 11, but for *pp* collisions at 40 TeV.

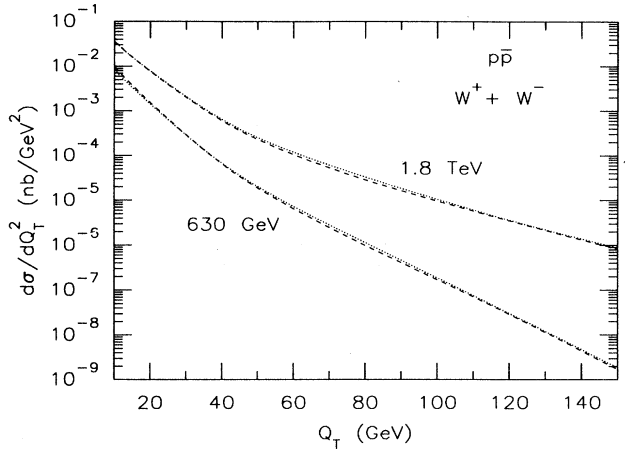

FIG. 14. Dependence on the choice of energy scale E_s. Dashed and dotted lines are for $E_s^2=Q_T^2$ and $E_s^2=Q^2$, respectively.

significant. It is apparent that the gluon contributions grow rapidly with $\sqrt{S}$, reflecting the rapid growth of the gluon density with the decreasing values of momentum fraction x that then become kinematically accessible. It is interesting that the gluon-gluon contribution tends to be negative, which implies that the collinear singularities dominate the *GG* process. However, it is apparent that the *GG* contribution is negligible at presently available energies.

4. *Scale dependence*

In Fig. 14 we illustrate the effect on the Q_T distribution of two choices for the "typical energy scale" E_s of the process: namely, $E_s^2=Q_T^2$ and $E_s^2=Q^2$. The choice of the former tends to yield a smaller cross section at larger values of Q_T: this is partly because the larger scale implies a smaller value of α_s. It is apparent, however, that the choice of scale is not significant given the uncertainties in the experimental data at larger values of Q_T. The ratio of the Q_T distributions with the two choices of scale has a rather complicated behavior as a function of Q_T, so we choose not to present a higher resolution plot than the one in Fig. 14.

In Figs. 15–18 we fix $E_s=Q_T$ and study the dependence of the differential cross section on the factorization and renormalization-scale factors ζ_M and ζ_μ which were defined in Eqs. (4.1) and (4.2).

We first discuss Fig. 15. The curve showing the ζ_μ dependence in lowest order simply reflects the change in α_s as the renormalization scale varies. The $O(\alpha_s^2)$ corrected cross section is almost independent of ζ_μ because the next-to-leading-order terms correct for the scale dependence in leading order (recall that the perturbation series summed to all orders is independent of the renormalization scale). The lowest-order curve in which $\zeta_\mu=\zeta_M$ shows a much stronger scale dependence than the curve with $\zeta_M=1$. The dependence on the factorization scale M arises solely from the parton densities $f_h^a(x,M^2)$ in lowest order. The corresponding $O(\alpha_s^2)$ corrected curve with $\zeta_M=\zeta_\mu$ also depends fairly strongly on the scale factor. The scale dependence of the nonsinglet cross sections was studied by Bawa and Stirling[10] who single out two scales: $\zeta^{\rm PMS}$ at which the corrected cross section has a maximum and $\zeta^{\rm FAC}$ at which the leading order and corrected cross sections are equal. $\zeta^{\rm PMS}$ is the scale at which the cross section is minimally scale dependent (locally). Loosely speaking, it approximates the "optimized" result in the sense of Ref. 30. $\zeta^{\rm FAC}$ represents the scale at which the perturbation expansion exhibits "fastest apparent convergence." It is apparent from the figure that both of these scales are smaller than unity, with $\zeta^{\rm PMS}$ the smaller of the two and comparable with the scale $\zeta_{\rm mom}$ appropriate to renormalization by momentum subtraction.[29] Also shown in the figure is the ζ_M dependence of the corrected cross section with $\zeta_\mu=1$. This curve has a much milder scale dependence than when the two scales are varied simultaneously. Figure 16 shows analogous curves at a higher value of Q_T. The behavior of these curves is similar to the corresponding curves in

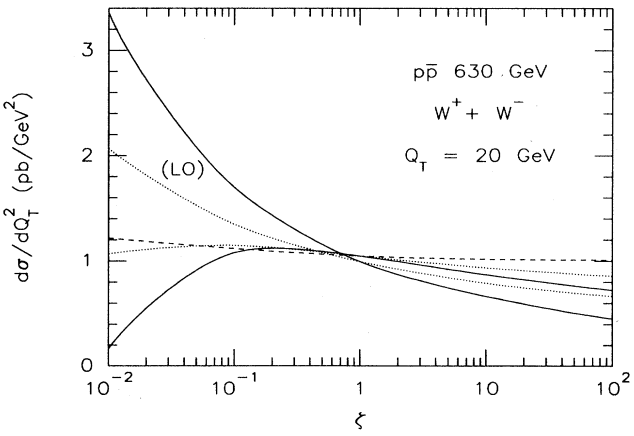

FIG. 15. Dependence on the renormalization scale factor ζ_μ and the factorization scale factor ζ_M. The solid curves are for $\zeta_\mu=\zeta_M=\zeta$, the dashed curve for $\zeta_M=\zeta$ with $\zeta_\mu=1$, and the dotted curves for $\zeta_\mu=\zeta$ with $\zeta_M=1$. Curves labeled (LO) represent $O(\alpha_s)$ contributions.

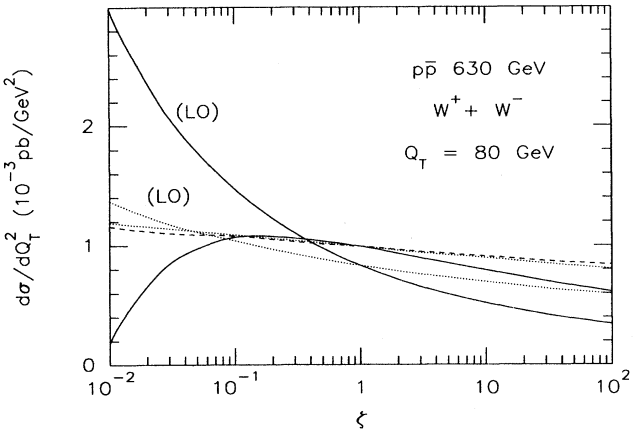

FIG. 16. Same as Fig. 15, but at $Q_T=80$ GeV.

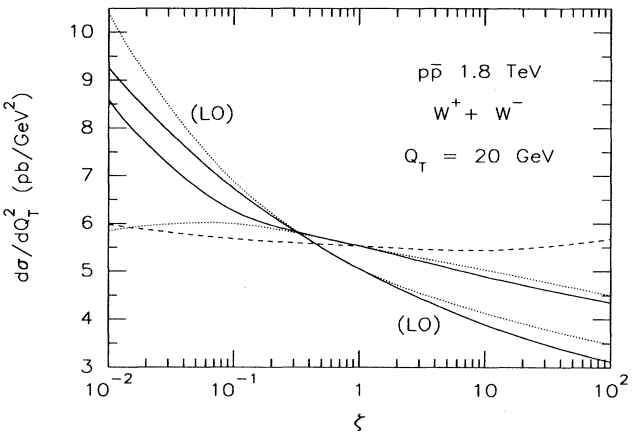

FIG. 17. Same as Fig. 15, but at $\sqrt{S}=1.8$ TeV.

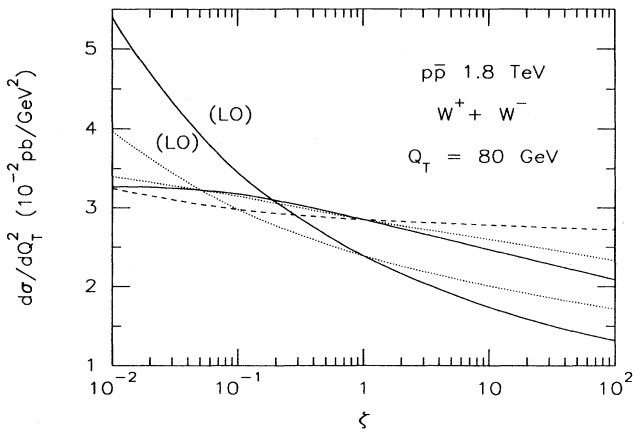

FIG. 18. Same as Fig. 15, but at $\sqrt{S}=1.8$ TeV and $Q_T=80$ GeV.

Fig. 15. The ζ_μ variation is milder because the coupling is evaluated at a larger scale.

Figures 17 and 18 exhibit the scale dependence of the cross section at $\sqrt{S}=1.8$ TeV. The scale dependence of the leading-order cross sections is similar to that at 630 GeV. However, the $O(\alpha_s^2)$ corrected cross sections behave somewhat differently especially at lower values of Q_T. Figure 17 shows that the $\zeta_M=\zeta_\mu$ curve at $Q_T=20$ GeV does not have an extremum in the range plotted: thus this curve cannot be used to determine $\zeta^{\rm PMS}$. Figure 18 shows that the curve does barely turn over at $Q_T=80$ GeV. This behavior suggests that the "optimum" scale factors should be determined by looking for a saddle point of the cross section as a function of the two variables ζ_M and ζ_μ. Indeed, an analysis of just this nature ha been done for prompt photon production at large Q_T (Ref. 34). The existence of a saddle point and its theoretical significance are not entirely clear when one is dealing with singlet cross sections which mix different initial-state partons.[35] Since the precise choice of scale does not appear to significantly affect the numerical comparison with experiment, we will not pursue the question of the optimal choice any further in this paper.

C. Conclusions

We have presented complete analytical cross-section formulas for inclusive electroweak boson production at large transverse momentum in next-to-leading order of QCD. The radiative corrections evaluated at an energy scale $E_s=Q_T$ appear to be well behaved for all $Q_T \geq 0.1\sqrt{Q^2}$. The optimum choice of scale in the $\overline{\rm MS}$ scheme appears to be $E_s \simeq 0.1-0.5Q_T$. We find that the qG process contributes on the order of one-half of the cross section at $\sqrt{S}=1.8$ TeV. The Q_T dependence of the qG contribution is slightly softer than that of the nonsinglet $q\bar{q}$ contributions, but this difference will not be easy to detect in the data. However, if the absolute cross section could be measured with sufficient accuracy at large Q_T, it would provide striking evidence for the qG contribution. Ultimately, this type of measurement could provide an independent means of determining the gluon density in the proton.

The principal conclusion of this study is that the inclusive cross section $d\sigma/dQ_i^2$ at large Q_T is reliably predicted by perturbative QCD at collider energies. Any large deviations from these predictions must signal new physics not contained in the standard theory.

There are three important respects in which this work is incomplete. The most important of them from a phenomenological standpoint concerns the region of $Q_T^2 \ll Q^2$ where the cross section is large and where large logarithms of Q_T^2/Q^2 need to be summed to obtain a reliable perturbation expansion. The other two are primarily of theoretical interest: the rigorous treatment of γ_5 in dimensionally regularized expressions, and the question of determining the optimal renormalization and factorization scales for the singlet cross sections. These questions are under study: the results will be presented in a future publication.[24]

ACKNOWLEDGMENTS

This calculation would not have been initiated or completed if it were not for R. K. Ellis and we would like to gratefully acknowledge our considerable indebtedness to him. Conversations with several colleagues, especially I. Hinchliffe, have proved helpful in this calculation. We thank W. J. Stirling for providing us with his numerical parton densities and for helpful instructions concerning their use. We thank P. B. Arnold and M. H. Reno for sending us an early copy of their paper and for several communications that were very helpful in comparing our respective analytical formulas and in expediting the completion of this work. Finally, we thank C. M. Hung for performing an independent calculation of the function D_{ab}. This work was supported in part by NSF Grants Nos. PHY-83-10883 and PHY-87-13231.

APPENDIX: CROSS-SECTION FORMULAS

In this appendix we present analytical formulas for the various invariant functions which were introduced in Eqs. (2.12), (2.17), (2.18), and (2.21) for the inclusive parton-level cross sections for production of $W^{\pm}$, Z^0 and γ^*.

The formulas presented here are functions of the invariants s,t,u,Q^2 and $s_2 \equiv s+t+u-Q^2$. In order to present these somewhat lengthy expressions in reasonably compact form, we define the frequently occurring denominator factors,

$$d_t=\frac{1}{s_2-t},\quad d_u=\frac{1}{s_2-u},\quad d_{st}=\frac{1}{s+t-s_2},$$
$$d_{su}=\frac{1}{s+u-s_2},\quad d_s=\frac{1}{s+Q^2-s_2}, \tag{A1}$$
$$d_{tu}=\frac{1}{tu-s_2Q^2},\quad \lambda=\sqrt{(u+t)^2-4s_2Q^2},$$

and some transcendental functions:

$$f_s=\ln\left[\frac{s}{Q^2}\right],\quad f_t=\ln\left[\frac{-t}{Q^2}\right],\quad f_u=\ln\left[\frac{-u}{Q^2}\right],$$
$$f_{s_2}=\ln\left[\frac{s_2}{Q^2}\right],\quad f_{M^2}=\ln\left[\frac{M^2}{Q^2}\right],\quad f_{\mu^2}=\ln\left[\frac{\mu^2}{Q^2}\right],$$
$$f_A=\ln\left[\frac{A}{Q^2}\right],\quad f_{st}=\ln\left[\frac{st^2}{Q^2(s_2-t)^2}\right],$$
$$f_{su}=\ln\left[\frac{su^2}{Q^2(s_2-u)^2}\right],\quad f_\lambda=\ln\left[\frac{s+Q^2-s_2+\lambda}{s+Q^2-s_2-\lambda}\right],$$
$$f_{stu}=\ln\left[\frac{sQ^2}{(s_2-t)(s_2-u)}\right],$$
$$f_{tu}=\ln\left[\frac{tu-s_2Q^2}{(s_2-t)(s_2-u)}\right], \tag{A2}$$
$$f_{\lambda t}=\ln\left[\frac{sQ^2(s_2-t)^2}{[s_2(2Q^2-u)-Q^2t]^2}\right],$$
$$f_{\lambda u}=\ln\left[\frac{sQ^2(s_2-u)^2}{[s_2(2Q^2-t)-Q^2u]^2}\right],$$
$$f_{1t}=\mathrm{Li}_2\left[\frac{Q^2}{Q^2-t}\right]+\frac{1}{2}\ln^2\left[\frac{Q^2}{Q^2-t}\right],$$
$$f_{2t}=\mathrm{Li}_2\left[\frac{Q^2}{s}\right]+\frac{1}{2}f_s^2+f_s\ln\left[\frac{-t}{s-Q^2}\right],$$
$$f_{1u}=\mathrm{Li}_2\left[\frac{Q^2}{Q^2-u}\right]+\frac{1}{2}\ln^2\left[\frac{Q^2}{Q^2-u}\right],$$
$$f_{2u}=\mathrm{Li}_2\left[\frac{Q^2}{s}\right]+\frac{1}{2}f_s^2+f_s\ln\left[\frac{-u}{s-Q^2}\right],$$

where the Euler dilogarithm is defined by

$$\mathrm{Li}_2(z)=-\int_0^z dz'\frac{\ln(1-z')}{z'}=\sum_{n=1}^{\infty}\frac{z^n}{n^2}, \tag{A3}$$
$$|z|\le 1 .$$

Note that quantities such as d_t, f_t, etc., are to be considered implicit functions of s, t, u, s_2, and Q^2, so that interchanging $t\leftrightarrow u$ implies interchanging $d_t\leftrightarrow d_u$, $f_t\leftrightarrow f_u$, etc.

A. Contributions from virtual-exchange diagrams

The contributions of the one-loop diagrams in Fig. 2 will be presented in this section. The formula in Eq. (A4) is due to R. K. Ellis, and that in Eq. (A7) is taken from Ref. 8. We have checked that they agree with the analytic continuation of the one-loop corrections to the process $e^+e^-\to q\bar{q}G$, for which there exist several calculations[17] including one by one of us. For convenience, we have included the contribution of the $\overline{\mathrm{MS}}$ renormalization counterterm, Eq. (2.14), in these expressions.

We first present the virtual contributions to the Compton process, Eq. (2.12):

$$B_1^{qG}(s,t,u,Q^2)=A^{qG}(s,t,u,Q^2)\left[-\frac{2C_F+C_A}{\omega^2}+\frac{1}{\omega}[3C_F-2C_Ff_u+\tfrac{11}{6}C_A+C_A(f_u-f_s-f_t)]-8C_F-C_Ff_u^2\right.$$
$$\left.-\frac{\pi^2}{3}(C_F-C_A)+\tfrac{1}{2}C_A(f_u^2-f_s^2-f_t^2)+C_A(\tfrac{11}{6}f_{\mu^2}+f_{1t}-f_{2t})\right]$$
$$+C_F\left[\frac{u}{t+u}+\frac{u}{s+u}+\frac{u+t}{s}+\frac{u+s}{t}\right]+\left[C_F\frac{4u^2+2ut+4su+st}{(s+u)^2}+C_A\frac{t}{s+u}\right]f_t$$
$$+\left[C_F\frac{4u^2+2su+4ut+ts}{(t+u)^2}+C_A\frac{s}{t+u}\right]f_s$$
$$+(2C_F-C_A)\left[2\left[\frac{u^2}{(s+t)^2}+\frac{2u}{s+t}\right]f_u-\frac{Q^2}{st}\left[\frac{s^2+t^2}{s+t}\right]\right.$$
$$\left.+\frac{u^2+(u+s)^2}{st}\left[f_{1t}+f_{1u}-f_tf_u+\frac{\pi^2}{2}\right]+\frac{u^2+(t+u)^2}{st}(f_{1u}-f_{2u})\right], \tag{A4}$$

$$B_2^{qG}(s,t,u,Q^2)=A^{qG}(s,t,u,Q^2)\frac{1}{3}\left[-\frac{1}{\omega}-f_{\mu^2}\right], \tag{A5}$$

$$B_3^{qG}(s,t,u,Q^2)=\left[\frac{u+Q^2}{u-Q^2}\right]\left[1-\frac{Q^2}{u-Q^2}f_u\right]. \tag{A6}$$

The function $A^{qG}(s,t,u,Q^2)$ is defined in Eq. (2.13), B_2 originates in the renormalization counterterm, and B_3 is the contribution of the two diagrams in Fig. 2 with triangular quark loops.

We next present the virtual contributions to the annihilation process, Eq. (2.18). While the Compton and annihilation processes might seem to be related by the simple interchange $s\leftrightarrow u$, care must be exercised in continuing the logarithms and dilogarithms since s and u are of opposite sign. This accounts for the differences in the terms proportional to π^2 in these two formulas. We have

$$B_1^{q\bar{q}}(s,t,u,Q^2)=A^{q\bar{q}}(s,t,u,Q^2)\left[-\frac{2C_F+C_A}{\omega^2}+\frac{1}{\omega}[3C_F-2C_Ff_s+\tfrac{11}{6}C_A+C_A(f_s-f_u-f_t)]-8C_F-C_Ff_s^2\right.$$
$$\left.+\frac{\pi^2}{6}(4C_F-C_A)+\tfrac{1}{2}C_A[f_s^2-(f_t+f_u)^2]+C_A(\tfrac{11}{6}f_{\mu^2}+f_{1t}+f_{1u})\right]$$
$$+C_F\left[\frac{s}{s+t}+\frac{s}{s+u}+\frac{s+t}{u}+\frac{s+u}{t}\right]+\left[C_F\frac{4s^2+2st+4su+ut}{(s+u)^2}+C_A\frac{t}{s+u}\right]f_t$$
$$+\left[C_F\frac{4s^2+2su+4st+tu}{(s+t)^2}+C_A\frac{u}{s+t}\right]f_u$$
$$+(2C_F-C_A)\left[2\left[\frac{s^2}{(u+t)^2}+\frac{2s}{u+t}\right]f_s-\frac{Q^2}{ut}\left[\frac{u^2+t^2}{u+t}\right]+\frac{s^2+(s+u)^2}{ut}(f_{1t}-f_{2t})\right.$$
$$\left.+\frac{s^2+(s+t)^2}{ut}(f_{1u}-f_{2u})\right], \tag{A7}$$

$$B_2^{q\bar{q}}(s,t,u,Q^2)=A^{q\bar{q}}(s,t,u,Q^2)\frac{1}{3}\left[-\frac{1}{\omega}-f_{\mu^2}\right], \tag{A8}$$

$$B_3^{q\bar{q}}(s,t,u,Q^2)=-\left[\frac{s+Q^2}{s-Q^2}\right]\left[1-\frac{Q^2}{s-Q^2}f_s\right]. \tag{A9}$$

B. Processes with two final-state partons

In this section we present the invariant functions which describe the contributions from the diagrams in Figs. 3, 4, and 5.

1. *The Compton process $qG \to VqG$*

The most complicated cross section is that due to the Compton process, Eq. (2.12) and Fig. 3. The following functions contribute to terms proportional to $\delta(s_2)$:

$$C_1^{qG}(s,t,u,Q^2)=A^{qG}(s,t,u,Q^2)\left[\frac{2C_F+C_A}{\omega^2}-\frac{1}{\omega}[3C_F-2C_Ff_u+\tfrac{11}{6}C_A+C_F(f_u-f_s-f_t)]\right.$$
$$+C_F[\tfrac{7}{2}+2f_{M^2}(f_u-f_A)+f_A^2-\tfrac{3}{2}(f_{M^2}+f_A)]$$
$$+C_A\left[\frac{\pi^2}{6}+\frac{1}{2}(f_s-f_t-f_u)^2+2f_t(f_{M^2}-f_A)\right.$$
$$\left.\left.+2f_A(f_s-f_u-f_{M^2}+f_A)-\tfrac{11}{6}f_{M^2}\right]\right], \tag{A10}$$

$$C_2^{qG}(s,t,u,Q^2)=A^{qG}(s,t,u,Q^2)\frac{1}{3}\left[\frac{1}{\omega}+f_{M^2}\right]. \tag{A11}$$

The following terms contribute for nonzero values of s_2:

$$C_3^{qG}(s,t,u,Q^2)=\left[-\frac{s}{t}-\frac{t}{s}-\frac{2uQ^2}{st}\right]\left\{\left[\frac{f_{s_2}}{s_2}\right]_{A+}(2C_F+4C_A)\right.$$
$$+\left[\frac{1}{s_2}\right]_{A+}\left[C_F\left[-\frac{3}{2}+f_{su}+2f_{tu}-2f_{M^2}+\frac{t+u}{\lambda}f_\lambda\right]\right.$$
$$\left.\left.+C_A\left[2f_{stu}+\frac{f_{st}-f_{su}}{2}-f_{tu}-2f_{M^2}\right]\right]\right\}$$
$$+\frac{1}{s_2}\left[C_F-\frac{C_A}{2}\right]\left[\frac{s+2u}{t}\left[\frac{t+u}{\lambda}f_\lambda+f_{su}\right]+\frac{2t+4u}{s}f_{tu}\right]$$
$$+\frac{f_\lambda}{\lambda^3}\left\{C_F\left[\frac{3s}{4\lambda^2}(s+Q^2-s_2)(u^2-t^2)\left[1-\frac{u}{t}\right]+(u^2-t^2)\left[\frac{Q^2-s_2}{4s}+\frac{11}{4}+\frac{s_2}{t}-\frac{u}{2t}\right]\right.\right.$$
$$\left.-2s\left[t+\frac{u^2}{t}\right]-\frac{s}{2}(s-s_2)\left[\frac{u}{t}-3\right]+4s_2(t-u)+5su\right]$$
$$\left.+C_A\left[1-\frac{u}{t}\right]\left[\frac{t+u}{4}(s+Q^2-s_2)+s(s-s_2)\right]\right\}$$
$$+\frac{f_\lambda}{\lambda}\left\{C_F\left[\frac{t-u-2s_2}{4s}+\frac{11s-2u-4s_2}{4t}+\frac{2}{s}\left[1+\frac{u}{t}\right](5Q^2+s_2)-\frac{16Q^2s_2}{st}\right]\right.$$
$$\left.-\frac{C_A}{2}\left[\frac{t+u}{2t}+5\left[\frac{u}{s}-\frac{u+s_2}{t}\right]-\frac{7}{t}\left[s+\frac{us_2}{s}\right]+\frac{3}{s}(t-3s_2)+\frac{2}{st}(u^2+3s_2^2)\right]\right\}$$
$$+\frac{1}{\lambda^2}\left\{C_F\left[\frac{3s}{2\lambda^2}(t-u)^2\left[1+\frac{u}{t}\right]+\frac{s}{2t}(u-3t)+\left[1-\frac{u}{t}\right]\left[s_2-\frac{7u}{4}\right]\right.\right.$$
$$\left.\left.+(t-u)\left[\frac{11}{4}+\frac{3t+3u}{2s}-\frac{2s_2}{s}\right]\right]+C_A\left[\frac{u}{t}-1\right](s+s_2)\right\}$$
$$+2d_t^3st[4C_F-3C_A-(C_F-C_A)(f_{s_2}-f_{M^2})]$$
$$+d_t^2\{C_F(3s-8t-4u)-C_A(9s-4t+4u)+2(f_{s_2}-f_{M^2})[C_F(t+u)+C_A(3s+2u)]\}$$

$$
\begin{aligned}
&+d_t\left\{\left[C_F(f_{s_2}-f_{M^2})-C_A\left[f_{s_2}-f_{M^2}+\frac{f_{stu}+f_{s_2}-f_{tu}}{2}+\frac{f_{st}+f_{\lambda t}}{4}\right]\right]\right.\\
&\quad\times\left[4\left[1+\frac{u}{s}\right]\left[1-\frac{u}{t}\right]-2\left[\frac{s}{t}+\frac{t}{s}\right]\right]-C_F(f_{s_2}-f_{M^2})\frac{s+2u}{t}\\
&\quad+C_A\left[(2f_{\lambda t}+2f_{st})\frac{u+s}{t}+2(f_{s_2}-f_{M^2})\left[\frac{5s+4u}{t}-2\right]\right]\\
&\quad\left.-C_F\left[4+\frac{s-2u}{t}+\frac{2u-3t}{s}-\frac{u^2}{st}\right]+C_A\left[7-\frac{3s+2u}{t}\right]\right\}\\
&+d_u\left[2C_F\left[f_{M^2}-f_{s_2}-\frac{s}{t}\right]+C_A\left[\frac{s}{t}-1\right]\right]\\
&+d_{st}C_F(f_{su}-2f_{tu}-f_{\lambda t})\left[1-\frac{s_2}{t}\right]\frac{s_2^2-2u(s_2-u)}{s^2}\\
&+d_{tu}C_F\left\{2(f_{M^2}-f_{s_2}-f_{tu})\left[\frac{2s}{t}(Q^2+2u)+t-s_2+\frac{4u}{t}(2u-s_2)\right.\right.\\
&\qquad\left.+\frac{2}{s}(u-s_2)\left[t-2u+\frac{2u^2}{t}\right]\right]+s_2-t+4u\left[\frac{Q^2}{t}+\left[1-\frac{u}{t}\right]\frac{t-Q^2}{s}\right]\Bigg\}\\
&+C_F\left\{\frac{1}{st}\left[\frac{2u(s_2-u)-s_2^2}{s}-s_2\right](f_{su}-2f_{tu}-f_{\lambda t})-2\left[\frac{1}{t}-\frac{2}{s}+\frac{4u}{st}\right]f_{tu}\right.\\
&\quad+\frac{u-3s_2+5Q^2}{st}f_{\lambda t}+\left[\frac{5}{s}+\frac{1}{u}\left[1+\frac{2t}{s}-\frac{3s_2}{s}\right]-\frac{s_2Q^2}{su^2}\right]f_{su}\\
&\quad+\left[\frac{8}{s}+\frac{3}{t}+\frac{1}{u}-\frac{4u}{st}+\frac{2t-3s_2}{su}-Q^2\left[\frac{1}{t^2}+\frac{s_2}{su^2}\right]\right](f_{s_2}-f_{M^2})\\
&\quad\left.-\frac{2}{s}+\frac{3}{4t}-\frac{1}{u}+\frac{3u}{st}-\frac{t+s_2}{su}+Q^2\left[\frac{s_2}{su^2}-\frac{1}{2t^2}\right]\right\}\\
&+C_A\left\{2(f_{s_2}-f_{M^2})\left[\frac{6}{s}-\frac{2}{t}-\frac{2Q^2}{st}-\frac{3s_2}{st}\right]+\left[\frac{15}{2s}-\frac{9s_2}{2st}-\frac{2Q^2}{t^2}\right]f_{st}\right.\\
&\quad+2\left[\frac{1}{t^2}\left[s+\frac{s_2^2}{s}\right]+\frac{2s_2Q^2}{t^3}-\frac{4Q^2}{st}\left[1-\frac{Q^2}{t}\right]+\frac{2s_2Q^2}{st^2}\left[1-\frac{s_2}{t}\right]\left[1-\frac{Q^2}{t}\right]\right](f_{s_2}-f_{M^2}+f_{st})\\
&\quad+\frac{1}{s}\left[4-\frac{2u}{t}-\frac{s_2}{t}\right]\left[f_{s_2}+f_{stu}-\frac{f_{st}+f_{su}}{2}\right]+\frac{1}{s}\left[1-\frac{u}{t}\right]f_{su}\\
&\quad+\frac{1}{s}\left[\frac{2u}{t}-1\right]f_{tu}-2\left[\frac{3}{t}+\frac{1}{s}+\frac{2}{st}(u-s_2)\right]f_{\lambda t}-\frac{1}{s}-\frac{1}{t}+\frac{2s_2}{st}\\
&\quad+\frac{1}{t^2}\left[3Q^2+4s_2\left[1-\frac{3Q^2}{t}\right]\right]-\frac{2}{t^2}\left[s+\frac{s_2^2}{s}\right]\\
&\quad\left.+\frac{2Q^2}{st}\left[1-\frac{Q^2}{t}\right]-\frac{12s_2Q^2}{st^2}\left[1-\frac{s_2}{t}\right]\left[1-\frac{Q^2}{t}\right]\right\}. \qquad \text{(A12)}
\end{aligned}
$$

We note that the terms proportional to $1/s_2$ on the fourth line in Eq. (A12) are finite in the limit $s_2=0$, i.e., all singular terms which need to be defined as $A+$ distributions are proportional to the lowest-order cross section.

2. *The gluon-fusion process $GG \to Vq\bar{q}$*

The following function contributes to the gluon-fusion cross section, Eq. (2.17):

$$
\begin{aligned}
C^{GG}(s,t,u,Q^2)=&C_A\frac{d_s f_\lambda}{\lambda}\left[\frac{t^2}{\lambda^2}\left[\frac{3}{2\lambda^2}(2s-t-u)(u^2-t^2)+2s-3t+u+\frac{t^2-u^2}{s}\right]-\frac{3s}{2}-t\left[\frac{9}{2}+\frac{5t}{s}+\frac{3u}{s}\right]\right]\\
&+C_A\frac{f_\lambda}{\lambda}\left[\frac{t^2}{\lambda^2}\left[\frac{3}{2\lambda^2}(u^2-t^2)+1\right]\frac{Q^2-s_2}{s}-\frac{11}{4s}(Q^2-s_2)-4\left[1+\frac{t}{s}\right]\right]\\
&+C_F\frac{f_\lambda}{\lambda}[2d_s(t+u-2s)+6]+C_A\frac{t}{\lambda^2}\left[\frac{3(t-u)^2}{\lambda^2}\left[1+\frac{t+u}{2s}-2sd_s\right]\right.\\
&\qquad\left.+d_s(2s-3t+3u)-1-\frac{u}{s}+\frac{s_2(t-u)}{s^2}\right.\\
&\qquad\left.+\left[d_s-\frac{1}{2s}\right]\frac{(t-u)^2}{s}\right]\\
&+4C_F d_{tu}\left\{(f_{s_2}-f_{M^2}+f_{tu})\left[\frac{s}{2}+2t\left[1+\frac{t}{s}\right]\right]-t\left[1+\frac{t+u}{s}\right]\right\}\\
&+2d_s\left\{(C_A-2C_F)\frac{d_t t^2}{s}(f_{st}+f_{\lambda t})+C_F d_{st}(f_{su}-f_{\lambda t}-2f_{tu})\left[s+2u\left[1+\frac{u}{s}\right]\right]\right\}\\
&+d_s\left\{2C_F\left[f_{st}-\left[3+\frac{4(t+u)}{s}\right]f_{\lambda t}-\left[4+\frac{8t}{s}\right]f_{tu}\right]+\frac{C_A}{2}\left[(f_{st}+f_{\lambda t})\left[2+\frac{u+3t}{s}\right]\right.\right.\\
&\qquad\left.\left.+1+\frac{t(t-u)}{s^2}\right]\right\}\\
&+2C_F d_{st}(2f_{tu}+f_{\lambda t}-f_{su})\left[2+\frac{t+u}{s}\right]+8td_t^2[C_F(1-f_{s_2}+f_{M^2})+C_A]\\
&+(4C_F-2C_A)d_t d_u\frac{tu}{s}(f_{s_2}-f_{tu}+f_{stu})\\
&+d_t\left\{(C_A-2C_F)\left[\left[2+\frac{t+u}{s}\right](f_{st}+f_{\lambda t})+\frac{2}{s}(u-t)(f_{s_2}+f_{stu}-f_{tu})\right]\right.\\
&\qquad\left.-8C_F(f_{s_2}-f_{M^2}-1)+4C_A\left[2+\frac{u-t}{s}\right]\right\}\\
&+C_F\left\{2(f_{s_2}-f_{M^2})\left[\frac{2}{s}-\frac{2}{t}-\frac{1}{st}\left[u+\frac{s_2Q^2}{t}\right]\right]+\frac{4}{s}(f_{s_2}+f_{stu})-\frac{2}{t}\left[2+\frac{1}{s}\left[u+\frac{s_2Q^2}{t}\right]\right]f_{st}\right.\\
&\qquad\left.+\frac{1}{st}\left[4Q^2\left[1+\frac{s_2}{t}\right]-2u\right]\right\}-\frac{C_A}{s}\left[2(f_{s_2}+f_{stu})+\frac{f_{st}}{2}+\frac{5}{2}f_{\lambda t}+\frac{15}{4}\right].
\end{aligned}
\tag{A13}
$$

3. *The process $q\bar{q} \to VGG$*

The following formulas for the $q\bar{q}$ annihilation cross sections are taken from Ref. 8. We have recalculated them ourselves. They contribute to Eq. (2.18):

$$C_1^{q\bar{q}}(s,t,u,Q^2)=A^{q\bar{q}}(s,t,u,Q^2)\left[\frac{1}{\omega^2}(2C_F+C_A)-\frac{1}{\omega}[3C_F-2C_Ff_s+\tfrac{11}{6}C_A+C_A(f_s-f_u-f_t)]\right.$$
$$+C_A(\tfrac{67}{18}-\tfrac{11}{6}f_A+f_A^2)+C_F(2f_t+2f_u-4f_A-3)f_{M^2}$$
$$\left.+\left[C_F-\frac{C_A}{2}\right]\left[\frac{\pi^2}{3}+(2f_A+f_s-f_t-f_u)^2\right]\right], \tag{A14}$$

$$C_2^{q\bar{q}}(s,t,u,Q^2)=\frac{1}{2}\left[\frac{u}{t}+\frac{t}{u}+\frac{2Q^2s}{tu}\right]\left[\left[\frac{f_{s_2}}{s_2}\right]_{A+}(8C_F-2C_A)\right.$$
$$\left.+\left[\frac{1}{s_2}\right]_{A+}[-\tfrac{11}{6}C_A+2C_F(f_{tu}-2f_{M^2})+(2C_F-C_A)(2f_{stu}-f_{tu})]\right]$$
$$+C_F\left[sd_t^2+2d_t-\frac{s}{tu}+d_{tu}\left[s_2+\frac{2Q^2(u-s_2)}{t}\right]-2d_tQ^2\left[\frac{1}{u}-\frac{1}{t}\right]\right]$$
$$+C_A\left[-\frac{11}{6}\frac{s}{tu}+\frac{d_t^2s^2}{u}\left[\frac{3s_2}{2t}-2\right]+\frac{2d_ts}{u}+\frac{Q^2}{3t^2}\right]$$
$$+(2C_F-C_A)\left[\frac{d_t}{u}(Q^2-u)^2\left[d_u-\frac{1}{t}\right](f_{stu}+f_{s_2}-f_{tu})+\frac{s-Q^2}{tu}(f_{stu}+f_{s_2})\right]$$
$$+f_{tu}\left[C_Fd_{tu}\left[\frac{4Q^2}{tu}(Q^2-t)^2+2(Q^2+s)-s_2\right]+C_F\frac{s_2-2s}{tu}-C_A\frac{Q^2}{tu}\right]$$
$$+C_F(f_{M^2}-f_{s_2})\left[d_{tu}\left[4(u-Q^2)-s_2-\frac{4Q^2}{tu}(u-Q^2)^2\right]+d_t^2(Q^2-u)-\frac{d_t}{t}(2Q^2-u)\right.$$
$$\left.-\frac{2}{t}+\frac{Q^2}{t^2}+\frac{4Q^2}{tu}\right]. \tag{A15}$$

4. *The process $q\bar{q}\to Vq\bar{q}$*

The functions $D(s,t,u,Q^2)$ represent contributions to Eq. (2.18) from the quark-antiquark processes in Fig. 4:

$$D_{aa}^{(0)}(s,t,u,Q^2)=A^{q\bar{q}}(s,t,u,Q^2)\left[\frac{1}{3}\left[\frac{1}{\omega}+f_A-\frac{5}{3}\right]\right], \tag{A16}$$

$$D_{aa}(s,t,u,Q^2)=\frac{1}{2}\left[\frac{u}{t}+\frac{t}{u}+\frac{2sQ^2}{tu}\right]\frac{1}{3}\left[\frac{1}{s_2}\right]_{A+}+\frac{1}{3}\left[\frac{s}{tu}-\frac{Q^2}{t^2}\right]. \tag{A17}$$

The following interference only contributes to Z^0 production:

$$D_{ab}(s,t,u,Q^2)=\frac{1}{2}\left\{\frac{f_\lambda Q^2}{\lambda t}\left[\frac{2s+t+u}{\lambda^2}\left[\frac{3s(t-u)^2}{\lambda^2}+u-t-s\right]-1\right]\right.$$
$$\left.+\frac{2s+t+u}{2\lambda^2t}\left[-\frac{3}{\lambda^2}(s+Q^2-s_2)(t-u)^2+3t-u+2s-2s_2\right]\right\}. \tag{A18}$$

The following function is taken from Eq. (C1) of Ref. 8 which contains two misprints: the group-theory factor should be $\frac{1}{2}$ and not C_F, and the sign of the $-2t$ term on the first line is incorrectly given:

$$D_{bb}(s,t,u,Q^2)=\frac{1}{2}\left\{\frac{d_s}{2}\left[\frac{u}{s}-1\right]-\frac{5}{4s}+\frac{1}{\lambda^2}\left[ud_s\left[-2s+\frac{3u}{2s}(t-u)+4u-2t\right]+\frac{u}{2s}(2s+2s_2+t-u)\right]\right.$$
$$+\frac{3u^2}{\lambda^4}(u-t)\left[d_s(2s-u-t)-\frac{s+s_2}{s}\right]+\frac{f_\lambda}{\lambda}\left[d_s\left[\frac{2u^2}{s}+\frac{5u}{2}+\frac{3s}{2}\right]+\frac{3}{4}+\frac{u}{s}-\frac{s_2}{2s}\right]$$
$$+\frac{f_\lambda}{\lambda^3}\left[u^2d_s\left[3u-t-\frac{u^2}{s}+\frac{t^2}{s}-2s\right]+\frac{u}{s}\left[2s_2t-ut-2s_2^2+4us_2-3u^2+2ss_2-us\right]\right]$$
$$\left.+\frac{f_\lambda}{\lambda^5}\left[3d_su^2(u^2-t^2)(s-Q^2)+\frac{3u^2Q^2}{s}(u-t)(u+t-2s_2)\right]\right\}, \tag{A19}$$

$$D_{ac}(s,t,u,Q^2)=\left[C_F-\frac{C_A}{2}\right]\left\{\frac{f_\lambda}{\lambda}\left[\frac{3s^2Q^2}{\lambda^4}(t-u)^2\left[\frac{1}{t}+\frac{1}{u}\right]+\frac{sQ^2}{\lambda^2}\left[\frac{5s}{t}-\frac{7s}{u}+\frac{4u}{t}-4\right]\right.\right.$$
$$+\frac{1}{s_2}\left[\frac{2s^2}{u}+\frac{Q^2(2s+u)-us}{t}\right]+\frac{2s_2-u}{t}-2\Bigg]$$
$$+\frac{3sQ^2}{\lambda^4tu}(2s_2-u-t)(t-u)^2+\frac{1}{\lambda^2}\left[s(s-s_2)\left[\frac{7}{u}-\frac{5}{t}\right]\right.$$
$$\left.+\frac{1}{2}\left[\frac{t}{u}-\frac{u}{t}\right](10s+t+3u-2s_2)+2s-2s_2\left[1-\frac{u}{t}\right]\right]$$
$$+\frac{d_ts^2}{u}\left[d_t+\frac{3}{t}\right]+\frac{f_{st}}{t}\left[\frac{1}{s_2}\left[\frac{2s^2}{u}+2s+u\right]-\frac{2Q^2}{t}\right]$$
$$\left.-\frac{1}{2u}+\frac{3}{2t}-\frac{3Q^2}{t^2}\right\}. \tag{A20}$$

This expression is actually finite in the limit $s_2=0$ and hence the $1/s_2$ factors do not have to be interpreted as + distributions:

$$D_{bc}(s,t,u,Q^2)=\left[C_F-\frac{C_A}{2}\right]\left[\frac{f_\lambda}{\lambda}\left[\frac{6ss_2Q^2}{\lambda^4t}(t-u)^2\right.\right.$$
$$+\frac{1}{\lambda^2}\left\{2su+\left[s_2\left[1+\frac{t}{s}\right]-\frac{t}{2s}(t+u)\right](t+u)\left[1-\frac{u}{t}\right]+\frac{3s}{2}(t-u)\left[1-\frac{u}{t}\right]\right.$$
$$\left.-4s_2Q^2\left[1+\frac{s-u}{t}\right]\right\}+d_s\left[6s+2u+\frac{t^2-u^2}{2s}\right]-1$$
$$\left.+\frac{s+4u-2s_2}{2t}+\frac{3t+2u-6s_2}{s}+\frac{u^2-2us_2+4s_2^2}{st}\right]$$
$$+\frac{3s_2}{\lambda^4}(t-u)^2\left[1+\frac{u}{t}-\frac{2Q^2}{t}\right]+\frac{1}{\lambda^2}\left[-\frac{t}{2}+3u+s_2+\frac{t^2-u^2}{s}-\frac{u}{2t}(u+6s_2)\right]$$
$$+2d_t+d_s(f_{st}+f_{\lambda t})\left[\frac{2(s+u)}{t}+\frac{1}{2s}\left[t+\frac{u^2}{t}\right]\right]$$
$$+\frac{f_{st}}{2}\left[\frac{2}{t}+\frac{3}{s}+\frac{u-2s_2}{st}\right]+\frac{f_{\lambda t}}{2}\left[-\frac{2}{t}+\frac{1}{s}-\frac{u+2s_2}{st}\right]$$
$$\left.+\frac{1}{2t}-\frac{1}{s}+\frac{1}{st}\left[2u-\frac{4s_2Q^2}{t}\right]\right], \tag{A21}$$

$$D_{ad}(s,t,u,Q^2)=D_{ac}(s,u,t,Q^2)\ , \tag{A22}$$

$$D_{bd}(s,t,u,Q^2)=D_{bc}(s,u,t,Q^2)\ . \tag{A23}$$

The combined contributions of D_{ac}, D_{ad}, D_{bc}, and D_{bd} agree with Eq. (C3) of Ref. 8 in the case of γ^* production. For D_{cc} we have

$$D_{cc}(s,t,u,Q^2)=\frac{1}{2}\left\{\frac{f_\lambda}{\lambda}\left[\frac{s}{\lambda^2 t}(u^2-t^2)+\frac{3s+2u}{t}\right]+\frac{t+u-2s_2}{\lambda^2}\left[1-\frac{u}{t}\right]+d_t(f_{s_2}-f_{M^2})\left[sd_t+\frac{4s}{t}+\frac{2u}{t}\right]\right.$$
$$+(f_{st}-f_{M^2}+f_{s_2})\left[\frac{(s+s_2-Q^2)^2}{st^2}+\frac{1}{s}\left[\frac{u}{t}-\frac{2s_2Q^2}{t^2}\right]^2+\frac{4}{t}\left[\frac{Q^2}{t}-1\right]\right]+\frac{2f_{st}}{t}\left[1-\frac{Q^2}{t}\right]$$
$$\left.-d_t\left[sd_t-1-\frac{u}{t}\right]+\frac{2}{t}\left[\frac{u}{t}+s_2\left[\frac{1}{t}+\frac{1}{s}-\frac{s_2}{st}\right]\right]+\frac{1}{t}\left[\frac{Q^2}{t}-1\right]+\frac{12s_2Q^2}{st^3}\left[u-\frac{s_2Q^2}{t}\right]\right\}, \tag{A24}$$

$$D_{dd}(s,t,u,Q^2)=D_{cc}(s,u,t,Q^2)\ . \tag{A25}$$

In contrast with all the other D functions, the interferences between diagrams c and d yield different contributions depending on whether the handedness of the quark and antiquark are the same or opposite:

$$D_{cd}^{LL}(s,t,u,Q^2)=\frac{1}{2}\left\{\frac{f_\lambda}{\lambda}\left[-\frac{s}{\lambda^2 t}(t-u)^2+2d_s(s-t)+\frac{3s+2s_2}{t}-1\right]\right.$$
$$+\frac{u-2s_2}{\lambda^2}\left[\frac{u}{t}-1\right]+\frac{d_s d_{st}}{t}(f_{su}-f_{\lambda t}-2f_{tu})[2s(s+u)+u^2]$$
$$+d_s\left[(f_{st}-f_{tu})\left[1+\frac{u}{t}+\frac{2t}{u}+\frac{4s(Q^2+s_2)}{tu}\right]-(f_{\lambda t}+f_{tu})\left[1+\frac{u}{t}\right]\right]$$
$$\left.+d_{st}(2f_{tu}-f_{su}+f_{\lambda t})\left[1+\frac{2s+u}{t}\right]+\frac{2d_t s}{u}+\frac{f_{tu}}{tu}(s+s_2)-\frac{1}{t}\left[f_{st}+f_{\lambda t}+1-\frac{s}{u}\right]\right\}, \tag{A26}$$

$$D_{cd}^{LR}(s,t,u,Q^2)=\frac{1}{2}\left[\frac{2d_s s^2}{t}\left[d_{st}(f_{su}-f_{\lambda t}-2f_{tu})+\frac{2}{u}(f_{st}-f_{tu})\right]+d_{st}(2f_{tu}-f_{su}+f_{\lambda t})\left[1+\frac{2s}{t}-\frac{u}{t}\right]\right.$$
$$\left.+\frac{2}{tu}(f_{tu}-f_{su})(s+s_2-u)-\frac{2}{t}(f_{tu}+f_{\lambda t})\right]. \tag{A27}$$

5. *Quark-quark scattering $qq\to Vqq$*

The following functions $E(s,t,u,Q^2)$ represent contributions from the quark-quark processes in Fig. 5:

$$E_{aa}(s,t,u,Q^2)=E_{cc}(s,t,u,Q^2)=D_{cc}(s,t,u,Q^2)\ , \tag{A28}$$

$$E_{bb}(s,t,u,Q^2)=E_{dd}(s,t,u,Q^2)=D_{dd}(s,t,u,Q^2)\ . \tag{A29}$$

The two following equations are a consequence of the fact that when the antiquark in Fig. 4 is replaced by the quark in Fig. 5, the handed couplings change with the replacements $L\leftrightarrow -R^\dagger$. Thus the vector-vector contribution to the interference changes sign in going from Fig. 4 to Fig. 5, which is in accordance with Furry's theorem, while the axial-vector–axial-vector contribution does not. Thus the relationship between the quark-antiquark and quark-quark bd interferences given in Table 2 of Ref. 8 is in error by a minus sign:

$$E_{ab}^{LL}(s,t,u,Q^2)=E_{cd}^{LL}(s,t,u,Q^2)=-D_{cd}^{LR}(s,t,u,Q^2)\ , \tag{A30}$$

$$E_{ab}^{LR}(s,t,u,Q^2)=E_{cd}^{LR}(s,t,u,Q^2)=-D_{cd}^{LL}(s,t,u,Q^2)\ . \tag{A31}$$

The following two functions, when combined together, yield a result for γ^* production in agreement with Eq. (D1) of Ref. 8:

$$E_{ac}(s,t,u,Q^2)=\left[C_F-\frac{C_A}{2}\right]\left\{(f_{st}+f_{\lambda t})\left[\frac{4d_t d_s s^2}{t}-2d_t\left[1-\frac{u}{t}\right]-\frac{4}{t}\right]+\frac{4Q^2}{t^2}f_{st}\right\}, \tag{A32}$$

$$E_{ad}(s,t,u,Q^2)=\left[C_F-\frac{C_A}{2}\right]\left\{\frac{1}{s}(2f_{s_2}-f_{st}-f_{su}+2f_{stu})\left[-2-\frac{u}{t}-\frac{t}{u}+\frac{2s_2}{tu}(Q^2-s)\right]-\frac{2}{s}\left[2+\frac{u}{t}+\frac{t}{u}-2s_2Q^2\left[\frac{1}{t^2}+\frac{1}{u^2}\right]\right]\right\}, \tag{A33}$$

$$E_{bc}(s,t,u,Q^2)=E_{ad}(s,u,t,Q^2)\ , \tag{A34}$$

$$E_{bd}(s,t,u,Q^2)=E_{ac}(s,u,t,Q^2)\ . \tag{A35}$$

---

*Present address: Department of Physics, National Taiwan University, Taipei, Taiwan, Republic of China.

[1]C. Albajar *et al.*, Phys. Lett. B **198**, 271 (1987); G. Arnison *et al.*, Phys. Lett. **122B**, 103 (1983); M. Banner *et al.*, *ibid.* **122B**, 476 (1983).

[2]F. Abe *et al.*, Phys. Rev. Lett. **62**, 1005 (1989).

[3]S. D. Drell and T.-M. Yan, Phys. Rev. Lett. **25**, 316 (1970); Y. Yamaguchi, Nuovo Cimento **43A**, 193 (1966).

[4]W. A. Bardeen, H. Fritzsch, and M. Gell-Mann, in *Scale and Conformal Symmetries in Hadron Physics,* edited by R. Gatto (Wiley, New York, 1973); D. J. Gross and F. Wilczek, Phys. Rev. Lett. **30**, 1343 (1973); H. D. Politzer, *ibid.* **30**, 1346 (1973); G. 't Hooft (unpublished); K. G. Wilson, Phys. Rev. D **10**, 2445 (1974).

[5]S. L. Glashow, Nucl. Phys. **B22**, 579 (1961); A. Salam and J. C. Ward, Phys. Lett. **13**, 168 (1964); S. Weinberg, Phys. Rev. Lett. **19**, 1264 (1967).

[6]G. Altarelli, R. K. Ellis, and G. Martinelli, Nucl. Phys. **B157**, 461 (1979); J. Kubar-André and F. E. Paige, Phys. Rev. D **19**, 221 (1979); B. Humpert and W. L. van Neerven, Phys. Lett. **84B**, 327 (1979); A. P. Contogouris and J. Kripfganz, *ibid.* **84B**, 473 (1979), Phys. Rev. D **19**, 2207 (1979).

[7]C. Albajar *et al.*, Phys. Lett. B **193**, 389 (1987); R. Ansari *et al.*, *ibid.* **194**, 158 (1987); **215**, 175 (1988).

[8]R. K. Ellis, G. Martinelli, and R. Petronzio, Nucl. Phys. **B211**, 106 (1983).

[9]G. Altarelli, R. K. Ellis, and G. Martinelli, Z. Phys. C **27**, 617 (1985); G. Altarelli, R. K. Ellis, M. Greco, and G. Martinelli, Nucl. Phys. **B246**, 12 (1984).

[10]A. C. Bawa and W. J. Stirling, Phys. Lett. B **203**, 172 (1988).

[11]Using, e.g., the techniques in C. T. H. Davies and W. J. Stirling, Nucl. Phys. **B244**, 337 (1984).

[12]J. C. Collins and D. E. Soper, Nucl. Phys. **B193**, 381 (1981); **B194**, 4445 (1982); **197**, 446 (1982); J. Kodaira and L. Trentadue, Phys. Lett. **112B**, 66 (1982); **123**, 335 (1983).

[13]P. B. Arnold and M. H. Reno, Nucl. Phys. **B319**, 37 (1989); Report No. FERMILAB-PUB-89/59-T, 1989 (unpublished).

[14]R. K. Ellis, H. Georgi, M. Machacek, H. D. Politzer, and G. G. Ross, Nucl. Phys. **B152**, 285 (1979); D. Amati, R. Petronzio, and G. Veneziano, *ibid.* **B146**, 29 (1978).

[15]G. 't Hooft and M. Veltman, Nucl. Phys. **B44**, 189 (1972); C. G. Bollini and J. J. Giambiagi, Phys. Lett. **40B**, 566 (1972); J. F. Ashmore, Lett. Nuovo Cimento **4**, 289 (1972); W. J. Marciano, Phys. Rev. D **12**, 3861 (1975).

[16]G. 't Hooft, Nucl. Phys. **B61**, 455 (1973); W. A. Bardeen, A. J. Buras, D. W. Duke, and T. Muta, Phys. Rev. D **18**, 3998 (1978).

[17]R. K. Ellis, D. A. Ross, and A. E. Terrano, Nucl. Phys. **B178**, 421 (1981); K. Fabricius, I. Schmitt, G. Schierholz, and G. Kramer, Z. Phys. C **11**, 315 (1982); R. J. Gonsalves, Phys. Rev. D **34**, 1316 (1986).

[18]P. Breitenlohner and D. Maison, Commun. Math. Phys. **52**, 11 (1979); **52**, 39 (1979); **52**, 55 (1979); see also J. C. Collins, *Renormalization* (Cambridge University Press, Cambridge, England, 1984); for an application to an $O(\alpha_s^2)$ calculation, see J. G. Körner, G. Schuler, G. Kramer, and G. Lampe, Phys. Lett. **164B**, 136 (1985); Z. Phys. C **32**, 181 (1986).

[19]S. L. Adler, Phys. Rev. **177**, 2426 (1969); J. S. Bell and R. Jackiw, Nuovo Cimento **51**, 47 (1969).

[20]M. S. Chanowitz, M. A. Furman, and I. Hinchliffe, Nucl. Phys. **B159**, 225 (1979).

[21]G. Passarino and M. Veltman, Nucl. Phys. **B160**, 151 (1979).

[22]L. Rosenberg, Phys. Rev. **129**, 2786 (1963). In this early calculation, the correct result was obtained by imposing gauge invariance: with dimensional regularization, the correct gauge-invariant result emerges automatically.

[23]The contribution of these triangle diagrams with massive quarks to the total cross section for Z^0 production has been considered by D. A. Dicus and S. S. D. Willenbrock, Phys. Rev. D **34**, 148 (1986). Our results agree with theirs when the mass of the lighter quark in an SU(2) doublet is set to zero, and that of the heavier quark to ∞. We note that they have not included the contribution of the interference D_{ab}, Eq. (A18), which has the same flavor structure.

[24]R. J. Gonsalves and J. Pawłowski (in preparation).

[25]G. Altarelli and G. Parisi, Nucl. Phys. **B126**, 298 (1977).

[26]See Ref. 8. In Ref. 13 the deep-inelastic-scattering (DIS) scheme is used.

[27]A. D. Martin, R. G. Roberts, and W. J. Stirling, Phys. Rev. D **37**, 1161 (1988); Phys. Lett. B **206**, 327 (1988); Rutherford Report No. RAL-88-113, 1988, which describes the updated versions of the MRS B and E distributions used in this paper.

[28]In practice, the parton densities are extracted from particular processes using theoretical expressions that involve particular choices of renormalization scale and scheme, and thus acquire a hidden dependence on these choices. It is not obvious how this dependence can be minimized.

[29]W. Celmaster and R. J. Gonsalves, Phys. Rev. Lett. **42**, 1435 (1979); Phys. Rev. D **20**, 1420 (1979).

[30]P. M. Stevenson, Phys. Rev. D **23**, 2916 (1981); Nucl. Phys. **B203**, 472 (1982).

[31]G. Grunberg, Phys. Lett. **95B**, 70 (1980); Phys. Rev. D **29**, 2315 (1984).

[32]T. Appelquist and J. Carazzone, Phys. Rev. D **11**, 2856 (1986).

[33]These expressions differ from the results of Ref. 6, which generally use DIS factorization. In particular, the notorious large $(\frac{4}{3}\pi^2+1)$ term in the DIS K factor [coefficient of $\delta(1-z)$] is an appreciably smaller $(\frac{2}{3}\pi^2-8)$ in the $\overline{\text{MS}}$ scheme. We have recalculated the $\overline{\text{MS}}$ cross sections ourselves. Equation (4.1) agrees with the finite part of Eq. (89) of Altarelli *et al.* (Ref. 6), when $M^2=Q^2$; Eq. (4.2) differs from the finite part of Eq. (93) of Altarelli *et al.* (Ref. 6), a difference solely due to the fact that we have spin averaged over $n-2$ polarizations of the initial gluon while they average over 2 polarizations.

[34]P. Aurenche, R. Baier, M. Fontannaz, and D. Schiff, Nucl. Phys. **B297**, 661 (1988); **B286**, 509 (1987).

[35]H. D. Politzer, Nucl. Phys. **B194**, 493 (1982); P. M. Stevenson and H. D. Politzer, *ibid.* **B277**, 758 (1986).